FINAL REPORT

on

THE APPLICATIONS OF SKYLAB ALTIMETRY TO MARINE GEOID DETERMINATION

July, 1975

Principal Investigator: A. G. Mourad

Co-Investigators: S. Gopalapillai, M. Kuhner and D. M. Fubara

Z. H. Byrns, Code TF6 - NASA/JSC Technical Monitor

The research reported in this document was sponsored by the National Aeronautics and Space Administration, Lyndon B. Johnson Space Center, Houston, Texas, 70058, under contract NAS9-13276, EPN 440.

BATTELLE
Columbus Laboratories
505 King Avenue
Columbus, Ohio 43201

ACKNOWLEDGEMENT

The authors would like to acknowledge the cooperation and assistance of several NASA/JSC personnel, particularly Mr. Z. H. Byrns and Dr. Dean Norris. We are indebted to Mr. J. T. McGoogan of NASA/WFC for some of the preliminary Skylab altimetry and ephemeris data used, and for several helpful discussions on the S-193 systems characteristics. Appreciation is expressed to Mr. J. Marsh of NASA/GSFC and Dr. S. Vincent of WR&D, Inc.,for supplying the gravity anomaly data, and to Major D. DeLuchi of the DMA/Naval Hydrographic Center for providing the bathymetric maps used in the altimetry geoidal profiles correlation studies.

ABSTRACT

The overall objective of this investigation is to demonstrate the engineering feasibility of using satellite altimetry data for the determination of the Marine Geoid. This was acomplished by analyzing the altimetry data taken from four passes (#4, #6, #7, and #9) from the Skylab SL/2 mission. Basically, the approach to this analysis consisted of two steps. The first was to filter the noise from the altimetry data using the Generalized Least Squares Collocation technique. In the second step, the calibration constants and the marine geoid parameters along the satellite ground tracks were estimated by comparing the altimetry data with the a priori ground truth geoid.

The general mathematical model consisted of the linear relationship between the residual altitude from the altimetry data, the a priori geoid and the calibration constants. In this investigation only one constant term representing the cumulative effects of all the systematic errors is used as the calibration constant for each segment of data observed with different altimetry mode-submode combination. The resulting discontinuity in the geoidal profiles are removed by constraining the nearest ends of the adjacent segments.

The major results obtained in this investigation consist of some conclusions from the studies concerning the effects of errors inherent in the various input data, a set of bias terms for the various segments of the passes and a set of (altimetry) geoid profiles. For convenient study of correlations between these profiles with the existing bathymetry and gravity anomaly data, their corresponding profiles are also presented along with the geoidal profiles.

Detailed analysis of the results of these correlation studies as well as those of comparing computed geoidal profiles with a priori geoid are presented. Further applications of the altimetry data in the various fields of geodesy, geophysics and oceanography are also indicated.

The bias terms recovered for different segments are significantly different and have little or no correlation with each other. The general agreement between the altimetry and the a priori geoid profiles demonstrates the viability of the altimetry technique to determine the marine geoid. The short periodic deviations between them, considering their magnitudes, reflect the high frequency components of the geoid. It is also evident that the altimetry sensor is very sensitive to the local geoidal features such as those corresponding to trenches, ridges and sea mounts. Excellent agreement between the results obtained for the same place at different time (Passes #4 and #6 near the Puerto Rico trench) indicates the self consistency and precision of the altimeter except in the bias term. Pronounced correlations between the altimetry geoid and the existing bathymetry and gravimetry data can be the key to future applications of the altimetry.

LIST OF TABLES

LIST OF FIGURES
(Continued)

TABLE OF CONTENTS
(Continued)

LIST OF FIGURES

TABLE OF CONTENTS

FINAL REPORT

on

THE APPLICATIONS OF SKYLAB ALTIMETRY TO MARINE GEOID DETERMINATION

May, 1975

by

Principal Investigator: A. G. Mourad
Co-Investigators: S. Gopalapillai, M. Kuhner and D. M. Fubara
Z. H. Byrns, Code TF6 - NASA/JSC Technical Monitor

1.0 INTRODUCTION

This report covers activities performed by Battelle's Columbus Laboratories (BCL) on behalf of the National Aeronautics and Space Administration, Johnson Space Center (NASA/JSC), under contract No. NAS9-13276, EPN 440. BCL has the responsibility for "Calibration and Evaluation of Skylab Altimetry for Geodetic Determination of the Geoid".

The "Williamstown Study" [Kaula, 1970] recommended the use of spacecraft altimeters for geodetic, geophysical and oceanographic studies of the oceans and the earth's gravity field. An effort of this type was implemented for the first time in history under Skylab's experiment S-193, Stanley and McGoogan [1972]. The primary objective of the S-193 is to determine the engineering feasibility of the altimeter. The S-193 altimeter experiment is one of a number classified under "Earth Resources Experiments Package" (EREP) whose end objectives are to solve various problems on earth, that directly affect even the man in the street.

Three manned Skylab missions--SL/2, SL/3, and SL/4--were to provide data from the S-193 system. Geodetic analysis of Skylab S-193 altimeter data from mission SL/2 EREP pass numbers 4, 6, 7, and 9 is the subject of this report. The overall objective of the Battelle investigation is to demonstrate the feasibility of and necessary conditions in using the altimeter

data for the determination of the Marine Geoid (i.e., the geoid in ocean areas). The geoid is the equipotential surface that would coincide with "undisturbed" mean sea level of the earth's gravity field. "Undisturbed" is the condition that would exist if the oceans were acted on by the earth's force of gravity only and no other forces such as due to ocean currents, winds, tides, etc. Thus, determination of the geoid (mean sea level) is basic to the understanding of the oceans and their dynamic phenomena such as currents, tides, circulation patterns and,hence,air-sea interactions. Improved numerical weather predictions require accurate knowledge of these ocean dynamics phenomena. Navigation, waste disposal and pollution control also benefit from an accurate knowledge of ocean dynamics. More accurate determination of the geoid will lead to a better definition of the earth's gravity model. Computation of the global geoid by conventional methods is so expensive and time consuming and is beset with so many problems, as discussed in Fubara and Mourad [1972a], that these conventional techniques cannot be depended on for completion of the job in the foreseeable future. These factors justify the need for new systems and techniques. Current indications from the Skylab altimeter are that satellite altimetry may be the answer.

Figure 1-1 shows schematic geocentric relations of the various surfaces associated with satellite altimetry. TM is the raw altimeter range which has to be corrected for laboratory instrumental calibration, electromagnetic effects, sea state, and periodic sea surface influences to give TS. S represents the non-periodic "sea level". CT and CE, the geocentric radii of the altimeter and E, its subsatellite point on the reference ellipsoid, are computed from satellite tracking information. EG is the absolute geoidal undulation to be computed from this investigation, while SG is the quasi-stationary departure of the mean instantaneous sea surface from the geoid - the "undisturbed" mean sea level. It can be seen from the Figure 1-1 that the required geoidal undulations are given by

$$EG = ET - TM - MS - SG \qquad (1\text{-}1)$$

where, MS represents the sum of the calibration constants and the orbit uncertainties, if any. SG represents the deviation of the surface to which the measurement is made from the geoid. Since we do not have any information on SG which is not considered to vary significantly over the length of profiles corresponding to different submodes of observations, the sum (MS + SG) is considered as the calibration constant.

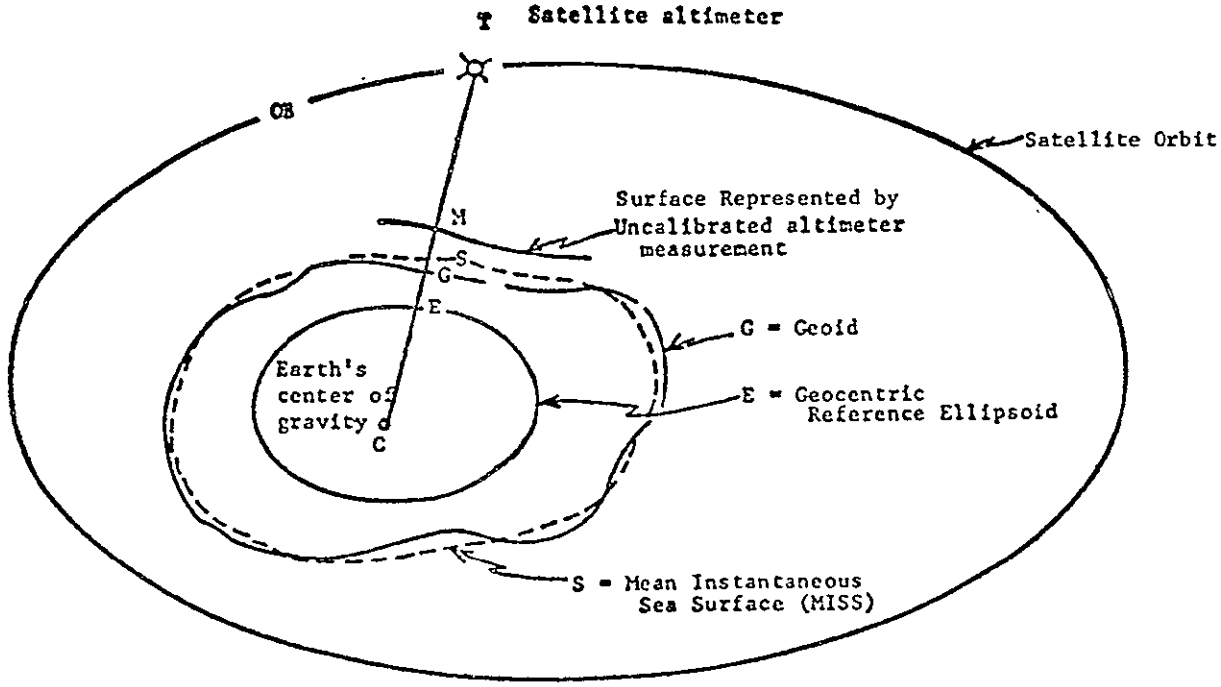

FIGURE 1-1. SCHEMATIC GEOCENTRIC RELATIONS OF SURFACES INVOLVED IN SATELLITE ALTIMETRY

The geoid to be determined must be in absolute position or geocentric (i.e., centered at the earth's center of mass) and have correct scale, shape and orientation in order to meet the goals of geodesy and also make contributions to the solution of problems in earth gravity modeling, geophysics, oceanography, etc. Correctness of shape depends on the precision of the altimeter and, in theory, absolute centering and orientation are dependent on the satellite orbit ephemeris. The correctness of geoid scale requires that the orbit ephemeris and the altimeter either have no biases or systematic errors, or that such biases and systematic errors must be known to an accuracy better than the error tolerance of the geoid to be computed. Currently and for some time to come, these two scalar conditions cannot be met because of unknown systematic errors or biases in tracking station geocentric coordinates, the earth's gravity model, the tracking systems and the altimeter itself. There is, therefore, a need for other sources of scale

and orientation control. Such a need can be satisfied by the use of terrestrial marine geodetic data to obtain scale and orientation control in the computation of the marine geoid (i.e., the geoid in the ocean areas) from satellite altimetry.

Three types of terrestrial geodetic parameters are required for this scale and orientation control: (1) The best available estimates of the figure of the earth in terms of the size and shape of a reference ellipsoid, (2) geoid heights referenced to this ellipsoid, and (3) marine geodetic controls. The first two of these are required as a priori inputs to provide a coarse scale. The third serves as benchmarks establishing the fine scale and misclosure errors. This is akin to leveling practice on land. Satellite altimetry is simply geodetic leveling from space.

Various estimates of the figure of the earth are in Mueller [1966] and Khan [1973]. The best space age estimates of the equatorial radius value range from 6,378,124 m [Strange et al, 1971] to 6,378,169 m [Veis, 1967], with most estimates in 6,378,140 $\pm$ 5 m range and a flattening of 1/298·255. Unfortunately, for the geoid, agreement and/or compatibility of various authors' geoids is considered very discouraging [Decker, 1972 and Fubara, et al, 1972a], particularly in the ocean areas. Vincent and Marsh [1973] geoid, based on equatorial radius of 6,378,142 m and flattening of 1/298·255 was selected for this investigation. A comparison of marine geoids of Vincent and Marsh [1973], Vincent, Strange and Marsh [1972] (see Figure 4-4) and Talwani, et al, [1972], shows why the choice of any of them can provide only coarse scale. The fine scale requires the use of marine geodetic control established via the use of satellite geodesy and astrogravimetric techniques [Fubara and Mourad, 1972a, 1972b and Fubara, 1973a, Mourad, et al, 1972a and 1972b]. Since there is no established marine geodetic control available at present, the geoid computed in this investigation will only have a coarse scale provided by the a priori geoid height input.

The primary results, conclusions and recommendations of this investigation are presented in Section 2.0 of this report. Formulations required for the data analysis are described in Section 3.0. Section 4.0 discusses the error analysis and validation experiments with preliminary data. The results of the actual data processing and analysis are given in Section 5.0.

Finally, in Section 6.0, the results of future applications and correlation studies between the altimetry geoid profiles and the existing gravity anomaly and bathymetric profiles are detailed.

PAGE INTENTIONALLY BLANK

2.0 SUMMARY OF RESULTS, CONCLUSIONS AND RECOMMENDATIONS

2.1 Program Summary

The overall objective of this investigation is to demonstrate the feasibility of and the necessary conditions in using satellite altimetry data for the determination of the Marine Geoid. This was accomplished by analyzing altimetry data taken from four passes (EREP passes #4, #6, #7, and #9) from the Skylab SL/2 mission. The obtained results indicate that these objectives were met successfully. The approach to this analysis consisted of two basic steps. The first step was to filter the noisy altimetry data using the Generalized Least Squares Collocation technique. In the second step, the filtered altimetry data were compared with the a priori ground truth geoid in order to determine the calibration constants and the altimetry geoid profile. This comparison was done essentially to have the altimetry geoid on the same scale as that of the a priori geoid.

The general mathematical model consists of the linear relationship between the residual altitude from the altimetry data, the a priori geoid, and the calibration constants. For the purpose of this investigation, only one constant term representing the cumulative effect of all the possible systematic errors associated with the residual altitude, is used as a calibration constant.

The only data of geodetic interest come from modes 1, 3 and 5 of the altimeter. Each of these modes consists of several submodes. Preliminary examination of these data indicated that the data from different submodes are associated with different biases. Consequently, different calibration constants have been used for different submodes of the altimeter. Least Squares techniques were used in the computation of these constants.

Use of different calibration constants for different submodes of observations caused discontinuity in the resulting altimetry geoid profiles. This situation is avoided by constraining the closest ends of the adjacent segments of the profiles to have the same value of undulation. The resulting altimetry geoid undulations are not the adjusted values i.e., altimetry observations plus the residuals to satisfy the

condition equation; but are the altimetry observations corrected for the computed biases only.

In an effort to compare the altimetry geoid profiles (2 sets: one from the unfiltered data, and the other from the filtered data, both of which are corrected for the bias terms) with the a priori ground truth geoid, all three sets of profiles are represented graphically as time series plots. On the same figures, profiles of the existing gravity anomalies and bathymetric data are presented to assess the correlations among the profiles in view of establishing the feasibility of the altimetry data in other applications.

2.2 Summary of Results and Conclusions

The major results obtained during this investigation can be divided broadly into two groups. One group is concerned with the effects of errors inherent in the various input data, such as the orbit ephemeris, a priori geoid etc. The other consists of the results of the actual analysis of the data from the Skylab EREP passes #4, #6, #7, and #9.

The results from the first group have been obtained from the analysis of some preliminary data from EREP pass #9 mode 5 (which were the only data available at the time the error analysis was carried out.) (These results are presented in section 4.0.) The second group of results consists of a set of recovered bias terms for each of the submodes of observations and a set of nine altimetry geoid profiles corresponding to the various passes and modes. Along with each of these profiles, the a priori geoid, gravity anomaly and the bathymetric data profiles are also presented for easy comparison. (Following are the summaries of specific results and recommendations based on analysis of the (1) preliminary data from EREP pass #9 mode 5 and (2) actual data from the various modes od EREP passes #4, #6, #7 and #9.

2.2.1 Analysis of Preliminary Data

(1) The analytical data handling formulations developed for this investigation appear to be very satisfactory. The required bias terms/ calibration constants and the geoid heights have been reliably determined.

(2) To ensure that the deduced calibration constants and the geodetic heights have the absolute scale, the use of geodetic control or a benchmark whose absolute geoidal height is known is indispensable.

(3) The a priori geoid inputs and the errors in them affect only the linear scale of the calibration constants and not the shape of the deduced geoid from the type of analytical processing used herein. In other words, the main effect of the a priori geoid input is reflected only in the scale of the geoid.

(4) The geodetic outcome of the satellite altimetry is extremely sensitive to the computed orbit. That is to say that the scale and orientation of the computed geoid highly depend on the orbit.

(5) Orbit computation in which inadequately calibrated altimeter ranges are employed as constraints is not desirable and present no advantage for processing altimeter data to compute the geoid. First, the unmodelled range biases introduce large systematic errors that are not admissible in Least Squares orbit computation. Such systematic errors can not be accurately eliminated through modeling unless some valid geodetic controls are used as constraints. Second, the geoid computed this way would be misleading due to the high correlation between the orbit and the geoid introduced by the inclusion of the altimeter ranges in the orbit computation.

(6) Deduction of a truly scaled geoid from satellite altimetry can not be achieved by merely subtracting altimeter ranges from the corresponding geodetic heights of the satellite unless every component of the altimetry measuring system and the computed orbit are error free.

2.2.2 Analysis of the Final Data from EREP passes #4, #6, #7, and #9

The results of the analysis of the altimetry data from the 4 passes, while confirming and reinforcing the conclusions already drawn from the analysis of the preliminary data, are used in making the following additional conclusions.

(1) The filtering technique described and applied in this investigation appears very effective in removing the noise from the altimetry data. Also, the procedure of estimating the calibration constants and geoid undulations has produced very satisfactory and realistic results. Specially, the simplified algorithm used in the computer programs for both the filtering and estimation processes has shown to be remarkable

with respect to its efficiency, simplicity, convenience and its adaptability to large scale data handling. Furthermore,the program used for the computer plot of the various profiles has demonstrated to be very useful.

(2) Even though altimetry heights were observed in several submodes of the altimeter, apparently, good and reliable data come only from submodes 0, 1, and 2 in modes 1 and 5 and from submodes 3, 4, and 5 in mode 3.

(3) The bias terms recovered for different segments (corresponding to submodes) of the same pass are significantly different. There appears to be very little or no correlation among the bias terms associated with the same submode.

(4) The agreement between the general slopes of the altimetry and ground truth geoid profiles demonstrate the viability of the altimetry technique in determining the marine geoid.

(5) Considering the magnitude of the deviations of the altimetry geoids from the conventional ground truth, it is evident that these deviations are mainly due to the high frequency components of the geoid rather than due to other causes.

(6) The skylab altimetry data analyzed in this investigation, have provided ample evidence that the altimetry sensor is very sensitive to local geoidal features such as trenches, ridges and sea mounts.

(7) In some of the profiles presented in Figures 5-4 thru 5-11, there appears to be some evidence of relative slopes between the altimetry and the ground truth geoids. Perhaps, these are due to the drift in the orbit or in the altimeter itself and have to be investigated further.

(8) Excellent agreement between the results obtained for the same place at different times (Puerto-Rico Trench area in passes 4 and 6 - Figure 5-12) shows that the satellite altimetry is self-consistent and precise. These results also show that the inherent biases, if any, can be successfully removed from the data.

(9) There are pronounced correlations between the altimetry geoid and the ocean bottom topography and gravity anomaly profiles. These correlations can be very useful in future applications such as in geology, geophysics, etc., of the altimetry data.

(10) The correlation between the altimetry geoid and the gravity anomaly and the topography profiles have been shown to be useful in resolving major discrepancies in the conventional geoid (e.g., pass #7, mode 5 over Puerto Rican Trench).

2.3 Recommendations

The following recommendations are based on the results of this investigation.

(1) Analysis of the rest of the data from SL/2 mission and also of all the data from SL/3 and SL/4 missions is necessary to obtain globally valid results and conclusions. The results obtained in this investigation have provided substantial information as to the feasibility of the technique, its accuracy, consistency, efficiency and speed in the determination of the marine geoid and to the application of the altimetry data in other areas. However, the amount of data analyzed in this investigation is only a small sample (on a very limited area of the globe) representing a fraction of the data collected during the three missions of the Skylab. Consequently, the results and conclusions obtained may be biased, having local but not global validity.

(2) Extensive correlation studies should be planned and carried out with sufficient ground truth data (gravity anomalies, bathymetric data etc.) in order to fully exploit the altimetry data. The apparent correlation between the altimetry geoid profiles and the existing gravity anomaly and bathymetric data profiles is so remarkable that it was possible to resolve the existing gross discrepancy between the ground truth and altimetry geoid profiles (Figure 5-8). The results of these correlations are very important for future applications in the areas of geology, geophysics etc. Further, the correlation study conducted in this investigation is rather limited mainly due to lack of resources and to our inability to collect, in time, sufficient uniform ground truth data. Consequently, a detailed investigation into these correlations will not only aid in verifying the altimetry data but also will provide additional informations towards future applications of the altimetry data.

(3) A program to investigate the feasibility of using geodetic control at sea should be planned and carried out in order to provide the geoid deduced from altimetry data from future missions with fine scale. This investigation clearly demonstrated that one of the practical ways of providing the altimetry geoid with fine scale is through such geodetic control.

(4) A program to investigate the feasibility of obtaining the ground truth geoid accurate to at least one meter should be planned and carried out. From the comparison of the altimetry and ground truth geoid profiles, it is apparent that the latter do not have the accuracy compatible with that attainable with an altimeter system similar to the one aboard the Skylab. If the objectives of the more sophisticated systems to be carried aboard future missions (such as GEOS-3 or SEASAT-A) are to be met, the ground truth requirements should be more stringent.

(5) Reanalysis of the data, used in this investigation with the detailed information on the various corrections to be made, should give better understanding of the recovered bias terms/calibration constants. The data used here have already been corrected for some causes of errors, e.g. time delay etc. Apparently, corrections for other sources such as pointing error, tropospheric refraction etc. have not been effected. However, due to the satellite arcs used being very short, the effects of these errors are constant over the whole length of an arc and will be absorbed into the calibration constants. Consequently, a reanalysis of the data will not affect the results of this investigation but will help to identify the true nature of the calibration constants if the other sources of errors are eliminated.

(6) Further investigations should be carried out to determine the exact cause of the apparent relative slope between the altimetry and the ground truth geoid profiles as can be seen from Figures 5-8, 5-10, and 5-11. The conjecture is that these slopes may be caused by drift in the radial component of the satellite position or in the altimetry measuring system itself. It may also be possible that the ground truth data are erroneous in that they may have a false orientation with respect to the actual geoid.

3.0 ANALYTICAL DATA HANDLING FORMULATION

3.1 Condition Equation of Intrinsic Parameters

The adjusted value R_i^a, corresponding to the measured altimeter range, R_i^o, is intrinsically related to (a) the geocentric coordinates, X_{si}, Y_{si}, Z_{si}, of the satellite at the instant of measurement, (b) the geoid undulation, N_i, referred to a given reference ellipsoid at the subsatellite point, and (c) the algebraic sum of the biases in all the measurement systems involved. The simplest geometry of these parameters is illustrated in Figure 3-1.

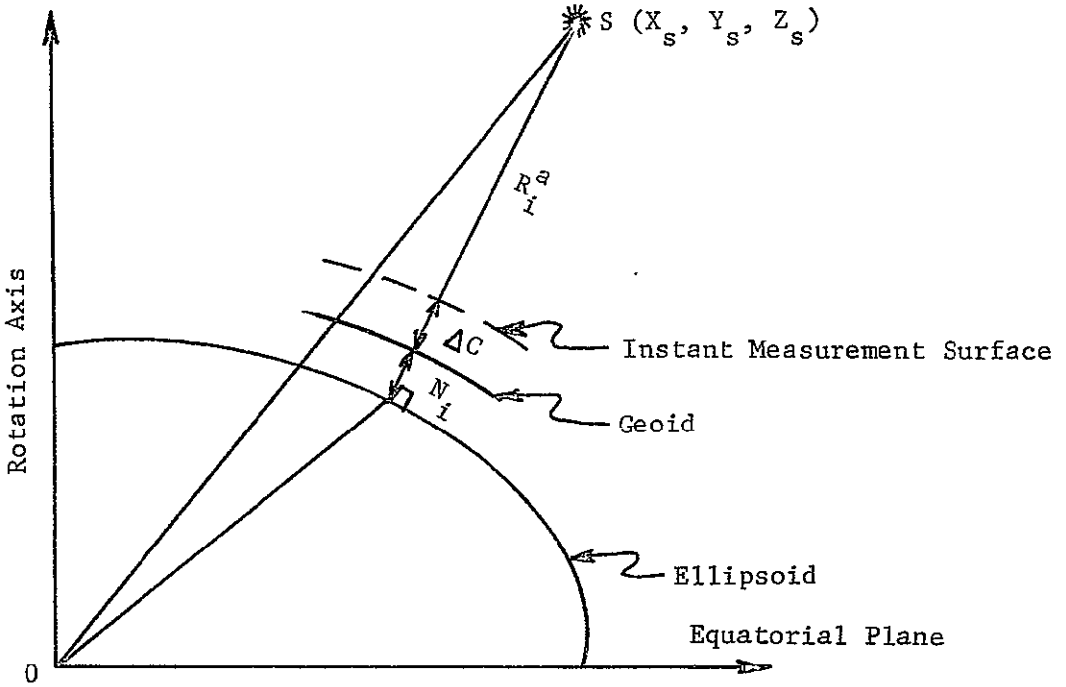

FIGURE 3-1. GEOMETRY OF THE INTRINSIC PARAMETERS INVOLVED IN AN ALTIMETRY MEASUREMENT

The general form of the condition equation between these parameters is given by

$$R_i^a + \Delta C + N_i - D_i = 0 \tag{3-1}$$

where ΔC is the total bias involved in the measurement and

$$D_i = F\ (X_{si},\ Y_{si},\ Z_{si},\ a,\ f) \tag{3-2}$$

being the height of the satellite above the reference ellipsoid given as a function of the geocentric coordinates of the satellite at the instant of

observation. a and f are the parameters (semi-major axis and flattening) defining the size and shape, respectively, of the assumed reference ellipsoid.

The function F in equation (3-2) is given explicitly by

$$D_i = (X_s^2 + Y_s^2)^{1/2} \operatorname{Sec} \varphi_i - a\,(1 - e^2 \operatorname{Sin}^2 \varphi_i)^{-1/2} \tag{3-3}$$

or

$$D_i = Z_s \operatorname{Cosec} \varphi_i - a(1 - e^2 \operatorname{Sin}^2 \varphi_i)^{-1/2}(1 - e^2) \tag{3-4}$$

where, e is the eccentricity of the reference ellipsoid, given by

$$e^2 = 1 - (1-f)^2 = 2f - f^2 \tag{3-5}$$

and φ_i is the geodetic latitude of the satellite position at the instant of measurement. φ_i is, usually, not known and has to be evaluated in an iterative cycle from the following equation.

$$\varphi_i = \tan^{-1} \left[\frac{Z_s + e^2 a (1 - e^2 \operatorname{Sin}^2 \varphi_i)^{-1/2} \operatorname{Sin} \varphi_i}{(X_s^2 + Y_s^2)^{1/2}} \right] \tag{3-6}$$

The first approximation for φ_i is given by

$$\varphi_i = \tan^{-1} \left[Z_s \, (X_s^2 + Y_s^2)^{-1/2} \right] \tag{3-7}$$

The bias ΔC is a function of the systematic errors arising from the (a) inaccuracies in the measurement itself, (b) deviation of the measured surface (instantaneous mean sea level) from the geoid, and (c) uncertainties in the geocentric position of the satellite. Two variations in the representation of ΔC has been considered in this investigation. In one, the bias is considered proportional to the measured range in which case, ΔC is given by

$$\Delta C = R_i \, \Delta c \tag{3-8}$$

where Δc is the calibration constant. In the other case, where ΔC is considered constant (independent of the range),

$$\Delta C = \Delta c \tag{3-9}$$

The variation in R_i is very small compared to R_i itself so that $R_i \Delta C$ remains constant for all practical purposes. This has been confirmed by the results of some preliminary studies with the Skylab altimetry data. Therefore, the model given by equation (3-1) will be used with equation (3-9) in the rest of this investigation.

At this point, some comments, as to why the cumulative effect of the systematic errors are represented only by a constant, may be appropriate. The major component of the error in the altimetry data is due to the uncertainties in the orbit computation. However, the lengths of the arcs, over which the Skylab altimetry data were taken, are very short, usually less than 3 minutes of time on the same altimeter mode. In each mode, the submodes have been changed several times and a quick look at the data indicated a change of bias whenever the submode was changed. Consequently, the length of arc, for which a constant bias term is considered, is usually less than even a minute of time. During such time interval the inaccuracies in the satellite ephemeris can be considered constant. On the other hand, inclusion of higher order terms such as first order drift or quadratic terms in time, will create a situation where any geoidal slope contained in the data will be absorbed by these parameters, unless there is sufficient information on these higher order terms so that they can be constrained to some a priori values.

Before proceeding to the discussion on the techniques and procedure used in the data analysis, some further comments on the compatibility of the height of the satellite above the ellipsoid and the a priori geoid undulations, is desirable. It is very important that these two quantities refer to the same reference ellipsoid. If they do not, they have to be made compatible by applying the necessary correction to either or both sets of quantities.

The difference between any two geodetic datums can be uniquely defined by a set of seven parameters. One such set is Δa, Δf, ΔX, ΔY, ΔZ, $\Delta\xi$ and $\Delta\eta$. Δa and Δf define the differences in size and shape of the reference ellipsoids; ΔX, ΔY, and ΔZ relate to the separation of centers of the ellipsoids; while $\Delta\xi$ and $\Delta\eta$ are angular separation of the respective minor and major axes of these ellipsoids. For most of the major datums, every effort is made to ensure that $\Delta\xi = \Delta\eta = 0$. However, this condition has never been exactly realized but its effect can be neglected for all practical purposes. It is also true, with most of the major datums, that they are geocentric which implies that $\Delta X = \Delta Y = \Delta Z = 0$. This leaves only a set of two parameters (Δa and Δf) with which to define the differences between the two reference ellipsoids. Then, the corresponding change in the height (Δh) above ellipsoid or in the undulation (ΔN) is given by

$$\Delta h = \Delta N = -\Delta a + a \, \mathrm{Sin}^2\varphi \cdot \Delta f \qquad (3\text{-}10)$$

where, φ is the geodetic latitude of the point under consideration.

3.2 General Approach to the Data Analysis

The purpose of this investigation, as mentioned earlier, is to determine the geoid along the altimetry profiles and to determine the calibration constants for the altimeter. This could be achieved by (1) filtering the noisy altimetry data,and (2) comparing them with the ground truth geoid to determine the calibration constants. The reason for such comparison is to have the altimetry geoid on the same scale as that of the ground truth assuming that the latter has the true scale. The scale error, if any, in the ground truth will automatically be transferred to the altimetry geoid. Theoretically, such a scale transfer could be done by having the comparison only at one point. However, the comparison was done at several points along the profile in order to minimize the effect of any systematic errors which may be associated with ground truth geoid computations.

Both the filtering and the estimation of calibration constants could be accomplished simultaneously if the ground truth geoid data are available for every altimetry data point. However, this is too difficult and uneconomical, if not impossible, due to the following reasons. The ground truth data used in this investigation are available in the form of a contour map on a scale of approximately 5^{o} to an inch. On this scale, the ground truth geoid data can be interpolated at intervals corresponding to the altimetry data at 5 seconds interval. Even if the ground truth is available for every altimeter data point, the inclusion of all the data points in the simultaneous filtering and estimation process will make the numerical handling of the data too difficult and uneconomical. Consequently, the following procedure has been adopted for the data analysis.

(1) The altimetry data are first filtered using the Least Squares Collocation technique. Only those data which belong to the same altimeter submode are included for simultaneous filtering.

(2) The ground truth data are obtained for every altimeter data point at 5 seconds intervals and are adjusted to obtain the calibration constants using the Least Squares estimation process. Here, all data from the same pass are included in a simultaneous adjustment/estimation.

(3) The geoid undulations are computed along the altimeter profile and plotted against time along with the ground truth geoidal plot for convenient comparison.

3.3 Filtering of the Altimetry Data

3.3.1 Principle of Generalized Least Squares Collocation (GLSC)

The Generalized Least Squares Collocation is a technique which combines filtering, estimation and prediction to give a solution which is optimal in the sense that it gives the most accurate results obtainable on the basis of the available data. The mathematical relationship that exists between the observations and the unknowns is assumed to be linear. In the event that the mathematical model is non-linear, it is linearised using Taylor's series expansion.

Let the observations, x, be modeled as follows [Moritz, 1972]

$$x = AX + s + n \tag{3-11}$$

where AX is a set of linear functions representing the systematic part of x with A and X being the design matrix and the unknowns respectively. s, a vector of systematic quantities which are random in nature, is called the "signal" and n, "the noise", is the vector of the measuring errors. This model is well illustrated in Figure 3-2.

We have to determine the curve shown on top (full line) by means of discrete observations (small circles), which are furthermore affected by observational errors n. These observations have to be filtered for the systematic parts AX and s, both of which are of importance. For example, in the case of the altimetry data, AX will represent the systematic errors identified and modeled, s will represent the geoid undulations, and n the observational errors.

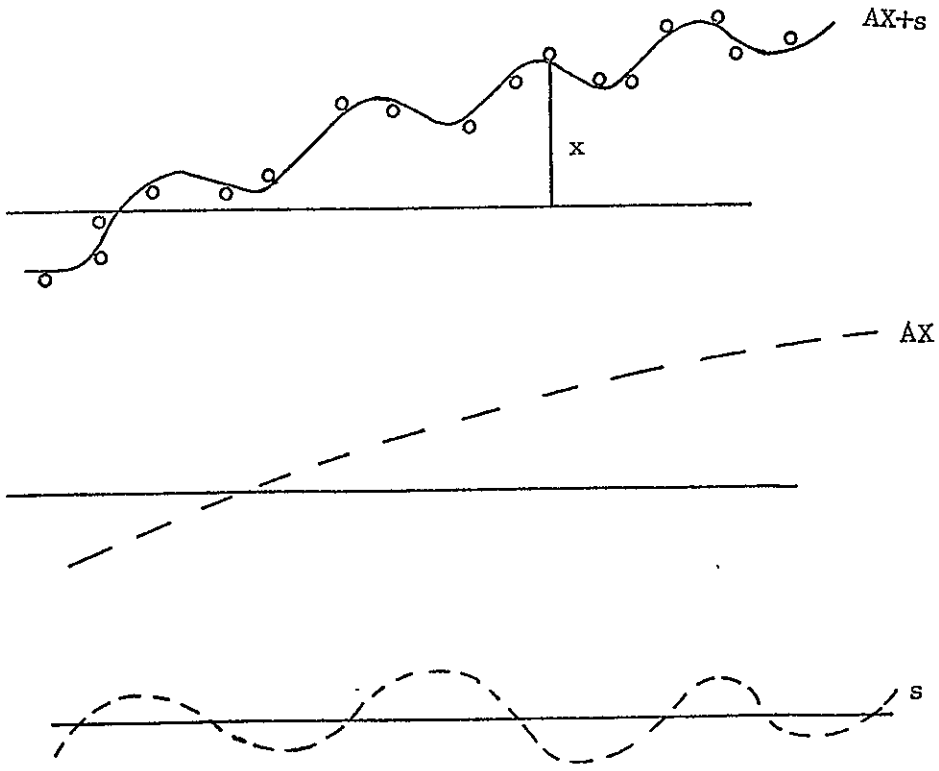

FIGURE 3-2. ILLUSTRATION OF A LEAST SQUARE COLLOCATION MODEL

If we consider the signal to be the short periodic deviations of the altimetry geoid from the ground truth geoid then AX will represent the combined effect of the systematic errors and the ground truth geoid undulations.

Determination of the parameters X is called estimation; computation of s at points other than the observation points is prediction and the removal of the noise, n, is filtering. Consequently, Least Squares Collocation is a combination of some or all of the above processes. In the following discussions, the application of this Collocation technique to the satellite altimetry data processing will be generalized to all three processes so that the formulas for one or two specific processes can be deduced from the general ones.

Let us assume that we wish to predict the signal, s, at an arbitrary number of "computation points" which may be different from the "data" points. Denote the number of such computation points by p and that of the data points by q. Define a vector v given by

$$v = [s^1_1 \; s^1_2 \; \ldots\ldots \; s^1_p \; z_1 \; z_2 \; \ldots \; z_q]^T = [s^{1T} \; z^T]^T \tag{3-12}$$

where,

$$z = s^1 + n \tag{3-13}$$

and T denoting the transpose. Consequently, v is a vector of p + q random variables that enter into the problem.

The covariance matrix Q of this vector v may be written as a partitioned matrix:

$$Q = \begin{bmatrix} C_{s^1_i s^1} & C_{s^1 z} \\ C_{z s^1} & C_{zz} \end{bmatrix} \tag{3-14}$$

Here,

$$C_{s^1 s^1} = \mathrm{Cov}\,(s^1, s^1)$$

denotes the covariance matrix of the signal s^1. Similarly, C_{zz} is the covariance matrix of the random vector z and C_{s^1z} and C_{zs^1} are the cross covariances between these quantities. Moritz (1972) has shown that

$$\begin{aligned} C_{zz} &= C_{xx} = C_{ss} + C_{nn} \\ C_{zs^1} &= C_{xs^1} = C_{ss^1} \\ C_{s^1z} &= C_{s^1x} = C_{s^1s}. \end{aligned} \tag{3-15}$$

Then, the matrix Q can be rewritten in the form

$$Q = \begin{bmatrix} C_{s^1s^1} & C_{s^1s} \\ C_{ss^1} & C_{ss} + C_{nn} \end{bmatrix} \tag{3-16}$$

Introducing the vector, v, as given by equation (3-12), equation (3-11) can be rewritten in the following form:

$$AX + BV - x = 0 \tag{3-17}$$

where

$$B = \begin{bmatrix} 0 & I \end{bmatrix} \tag{3-18}$$

which is a q by (q + p) matrix. Minimizing the squares V^TPV where,

$$P = Q^{-1} \tag{3-19}$$

with the side equation given by (3-17), the solution to our basic problems (estimation, filtering and prediction) are given by (Moritz, 1972)

$$X = (A^T\bar{C}^{-1}A)^{-1}A^T\bar{C}^{-1}x \tag{3-20}$$

$$V = QB^T\bar{C}^{-1}(x-AX) \tag{3-21}$$

and

$$s^1 = C_{s^1s}\bar{C}^{-1}(x-AX) \tag{3-22}$$

where,

$$\bar{C} = C_{ss} + C_{nn} \quad . \tag{3-23}$$

If the computation points for s and the data points are identical, then,

$$s^1 = s \tag{3-24}$$

and, from (3-22)

$$s = C_{ss}\bar{C}^{-1}(x - AX) \tag{3-25}$$

Consequently, the filtered observation $\bar{x}$ is given by

$$\bar{x} = AX + s \tag{3-26}$$

In order to evaluate these equations, all the matrices are known except the covariance matrices C_{ss} and C_{s^1s}.

These covariances describe the behavior of the signal in the coordinate frame in which the observations are made. For example, in the case of the satellite altimetry data, the frame is time which is in turn correlated with the latitude and longitude of points on the surface of the earth. If the signal is a set of geoid undulations, several empirical and numerical covariance functions are available [e.g., Tscherning and Rapp, 1974]. On the other hand, if the signal is a set of differences in undulations between the altimetry and the ground truth geoids, empirical or numerical covariance functions may be computed as described in [Moritz, 1972] using some sample altimetry and ground truth data in the area under investigations.

Some further comments about the evaluation of equations (3-20) to (3-22) may be appropriate at this point. There are two matrices, $(A^T\bar{C}^{-1}A)$ and $\bar{C}$, which need to be inverted. The size of the first matrix is the number (m) of unknowns in the X vector and that of the second matrix is q. For the problem to be over-determined, q must be greater than m. Consequently, if q is very large, the evaluation of these equations may become uneconomical and difficult if not impossible.

3.3.2 Implementation of GLSC in Filtering the Altimetry Data

Since the altimetry height which is the height of the satellite above the (instantaneous) mean sea level, is linearly related to the geoid undulation at the subsatellite point [Gopalapillai, 1974], the undulations, contaminated with the systematic and random errors, can be assumed to be the observations instead of the ocean-satellite distances. These observations which are denoted by N_{ai}, will be computed as follows:

$$N_{ai} = D_i - R_i^o \tag{3-27}$$

where, D_i and R_i^o are as given in equation (3-1). The subscript i refers to the i^{th} observation.

The altimetry observations given by equation (3-27) consist of three components; (1) a systematic bias, ΔC, (2) geoid undulations, N (signal) and, (3) a random component called noise, n, such that

$$N_{ai} = \Delta C + N_i + n_i \tag{3-28}$$

However, ΔC and N_i cannot be discriminated against each other without the ground truth data. Consequently, equation (3-28) is rewritten in the form

$$N_a = N_a^s + n \tag{3-29}$$

where

$$N_a^s = \Delta C + N \tag{3-29a}$$

The subscript, i, is left out to indicate that these equations are written in matrix form combining several equations of the form (3-28). Now, equation (3-29) is in a form similar to equation (3-11), where

$$\begin{aligned} X &= N_a \\ A &= 0 \\ s &= N_a^s \\ n &= n \end{aligned} \tag{3-30}$$

Then, the signal, N_a^s, is obtained by substituting equation (3-30) into equation (3-25):

$$N_a^s = C_{ss} \bar{C}^{-1} N_a \tag{3-31}$$

with

$$\bar{C} = C_{ss} + C_{nn} \tag{3-31a}$$

where C_{ss} is the autocovariance matrix of the undulations N, and C_{nn} is the covariance matrix of the noise. If the altimetry observations are assumed independent of each other then, C_{nn} is assumed to be diagonal in the following form:

$$C_{nn} = \sigma^2 I \tag{3-32}$$

where, σ^2 is the variance of a single observation and I is an identity matrix.

3.4 Estimation of Calibration Constants and the Geoid Profile

3.4.1 Observation Equation

The output from the filtering, as described in the previous section, is N_a^s whose components are given by equation (3-29a). The calibration constants are determined by comparing N_a^s with the ground truth geoid undulations, $\underline{N}$. The mathematical model for such comparison is obtained by rewriting (3-29a).

$$- N_a^s + \Delta C + N = 0 \quad . \tag{3-33}$$

This equation implies that the quantities N_a^s and N satisfy the equation only after the adjustment. Since we have a priori estimates (N_o) for N from the existing terrestrial data, we can consider equation (3-33) as a condition equation among observables with zero weights for ΔC, implying that we have no previous information on them. The system of observation equations resulting from such a set of condition equations can be written in a general form as

$$V + A V_x + W = 0 \tag{3-34}$$

where V are the residuals on $-N_a^s$ and V_x are the residuals on the a priori values of ΔC and N. The a priori values of ΔC can be assumed to be zero. The elements of the W matrix (vector) are computed from the corresponding elements of N_o and N_a^s as follows

$$W = N_o - N_a^s \tag{3-35}$$

Let the number of observation equations be n. Then, the structure of the matrices V, A, V_x, and W are illustrated in the following equations.

$$V = \begin{bmatrix} V_1 \\ V_2 \\ \vdots \\ V_i \\ \vdots \\ V_n \end{bmatrix} \tag{3-36}$$

$$A = \begin{bmatrix} 1 & 1 & & & & & \\ 1 & & 1 & & & 0 & \\ 1 & & & 1 & & & \\ 1 & & & & 1 & & \\ \cdot & & & & & \cdot & \\ \cdot & & & & & & \cdot \\ \cdot & & 0 & & & & \\ \cdot & & & & & & \cdot \\ 1 & & & & & & 1 \end{bmatrix} \tag{3-37}$$

$$V_x = \begin{bmatrix} \Delta C \\ \Delta N_1 \\ \Delta N_2 \\ \cdot \\ \cdot \\ \cdot \\ \Delta N_n \end{bmatrix} \tag{3-38}$$

$$W = \begin{bmatrix} W_1 \\ W_2 \\ \cdot \\ \cdot \\ \cdot \\ W_n \end{bmatrix} \tag{3-39}$$

ΔN_i, $i = 1, n$, in equation (3-38), are the residuals on the a priori estimates for the geoid undulations.

The systematic bias, ΔC, has been assumed to be constant for the entire altimetry data. This assumption is found unrealistic from the preliminary examination of the altimetry range observations from the Skylab mission. Every time the submode changed the bias appears to have been changing. Therefore, different bias terms have to be considered for different submodes. It should be emphasized, however, that the bias changes are associated with the change in the submodes and not with the submodes themselves. Consequently, the observation equation for the i^{th} observation which corresponds to the k^{th} submode (change), will be of the form

$$V_i + \Delta C_k + \Delta N_i + W_i = 0 \tag{3-40}$$

which will result in the A matrix of the form

$$A = \begin{array}{c} \begin{array}{ccccccccccc} \Delta C_1 & \Delta C_2 & \cdots & \Delta C_k & \Delta N_1 & \Delta N_2 & \cdot & \cdot & \cdot & \cdot & \Delta N_n \end{array} \\ \left[\begin{array}{ccccccccccc} 1 & 0 & 0 & 1 & & & & & & & \\ 0 & 1 & 0 & & 1 & & & & & & \\ 1 & 0 & 0 & & & 1 & & & & & \\ 0 & 0 & 1 & & & & 1 & & & & \\ \cdot & \cdot & \cdot & & & & & \cdot & & & \\ \cdot & \cdot & \cdot & & & & & & \cdot & & \\ \cdot & \cdot & \cdot & & & 0 & & & & & \\ 0 & 0 & 1 & & & & & & & & 1 \end{array}\right] \end{array} \tag{3-41}$$

while the structure of other matrices will remain unchanged.

Even if there is no submode change, it would be unrealistic to assume a constant bias for data from a very long pass. If the passes are very long, they should be broken up into short arcs and different bias terms have to be assumed for each of the subarcs. The observation equations (3-40) and (3-41) will also be ideally suitable for such a situation.

3.4.2 Least Squares Solution

Let the weight matrix for the altimeter observations be P, and that of the observable parameters, ΔC and N, be P_x. Then, the Least Squares solution for the system of observation equations [equation (3-40)] is given by

$$V_x = - \left(A^T P A + P_x\right)^{-1} A^T P W \tag{3-42}$$

$$V = - A V_x - W \tag{3-43}$$

where the superscript T indicates the transpose of the matrices.

The variance-covariance matrix, Σ_x, for the vector V_x is given by

$$\Sigma_x = \sigma_o^2 \left(A^T P A + P_x\right)^{-1} \tag{3-44}$$

with σ_o^2 being the variance of unit weight given by

$$\sigma_o^2 = \frac{\left(V_x^T P_x V_x + V^T P V\right)}{df} \tag{3-45}$$

where, df is the degree of freedom.

The fact that different bias terms have been used for the different segments of the data will result in a discontinuity in the computed geoid profiles. Therefore, it is necessary that the ends of these segments have to be properly constrained so that the resulting geoid will be realistically continuous.

3.4.3 Constraints for the Various Segments of the Geoid Profiles

In order to provide continuity along the geoid profiles, the geoid undulations at the closest ends of the adjoining segments of the profiles have to be constrained to be equal. However, the observations corresponding to these ends do not belong to the same point on the ocean surface. These observations are at about one second apart which corresponds to about eight kilometers. The geoid variation over this distance is well below the accuracy level of the altimeter observations. Therefore, it is reasonable to assume,

for all practical purposes, that the undulations at the nearest ends of adjoining segments are equal. This constraint can be expressed by an equation of the form

$$N_i - N_{i+1} = 0 \tag{3-46}$$

where the subscript i refers to the i^{th} observation (along the profile) which corresponds to the end of the first segment. In matrix notation, equation (3-46) can be rewritten in a form similar to equation (3-34) as

$$CV_x + W_c = 0 \tag{3-47}$$

where, V_x is given by equation (3-38). W_c is a vector of length equal to the number of constraints involved. Its elements are obtained by evaluating equation (3-46) with the a priori estimates of the geoid undulations. C is the design matrix for the constraints and will have the following structure

$$C = \begin{array}{c} \begin{matrix} \Delta C_1 & \Delta C_2 \ldots\ldots \Delta C_k & \Delta N_1 \ldots\ldots \Delta N_i & \Delta N_{i+1} \ldots\ldots \Delta N_j \ldots \Delta N_{j+1} \ldots \Delta N_n \end{matrix} \\ \begin{bmatrix} 0 & 0 \quad 0 & 0 \quad 1 & -1 \quad 0 \quad 0 & 0 \\ 0 & 0 \quad 0 & 0 \quad 0 & 0 \quad 1 \quad -1 & 0 \end{bmatrix} \end{array} \tag{3-48}$$

In this example for C, only two constraints have been assumed, but these can be any number of constraints depending on the number of segments in the profile. Usually it would be one less than the number of segments.

Now, there are two ways of incorporating these constraints into the matrix solution described in the previous section. One is to solve the two systems [equations (3-34) and (3-47)] simultaneously. The other approach is to solve the first system independently and then to make corrections for the constraints in a sequential solution. The first method is convenient and straightforward. However, due to some special characteristics (which would be discussed in Section 3.4.4) of the matrices involved in this solution, the second method is very economical. Consequently, the sequential solution approach is used here.

Let the solution for the unknowns described in equation (3-42) be denoted V_x^*. Then, the correction δV_x to V_x^* due to the addition of the constraints is given by

$$\delta V_x = N^{-1} C^T K_c \tag{3-49}$$

where,

$$N = \left(A^T P A + P_x\right) \tag{3-50}$$

$$K_c = -\left(C N^{-1} C^T\right)^{-1} \left(C V_x^* + W_c\right) \tag{3-51}$$

so that the new solution, V_x, is given by

$$V_x = V_x^* + \delta V_x \tag{3-52}$$

3.4.4 Special Characteristics of the Matrices Involved

The observations N_a^s and the a priori estimates for N (equation 3-33) are assumed to be independent. The biases corresponding to each of the submodes are also assumed to be independent of each other. Under these assumptions, the matrices P and P_x are diagonal. If the P_x matrix is partitioned along a line separating the biases from the undulations then, P_x can be written in the form

$$P_x = \left[\begin{array}{c|c} P_{x_1} & 0 \\ \hline 0 & P_{x_2} \end{array}\right] \tag{3-53}$$

Further, if the accuracy of all the observations in each of the groups N_a^s, N, and ΔC is assumed to be equal then,

$$P = p.I$$

$$P_{x1} = px_1.I \qquad (3\text{-}54)$$

$$\text{and } P_{x2} = px_2.I$$

where I is the identity matrix and p is the weight of a single observation. px_1 and px_2 have similar meanings for the bias and geoid parameters, respectively.

Partitioning (the matrix A) along the same line as in matrix P_x in equation (3-53), A can be rewritten in the form

$$A = \left[\begin{array}{c:c} A_1 & I \end{array}\right] \qquad (3\text{-}55)$$

where A_1 is the submatrix of A containing the columns corresponding to the bias terms ΔC_k. Similarly V_x is partitioned into components V_{x1} and V_{x2} such that

$$V_x = \begin{bmatrix} V_{x_1} \\ --- \\ V_{x_2} \end{bmatrix} \qquad (3\text{-}56)$$

Since the constraints are applied only to the geoid undulations, the matrix C can also be partitioned along the same line separating the bias parameters from the undulations. Let C_1 be the submatrix corresponding to the undulations. Then,

$$C = \left[\begin{array}{c:c} 0 & C_1 \end{array}\right] \qquad (3\text{-}57)$$

The special structures of these matrices, as described above, are taken advantage of in the numerical evaluation of equations (3-42) through (3-45) and equations (3-49) through (3-52).

3.4.5 Simplified Algorithm for Computer Processing of Altimetry Data

3.4.5.1 Solution of the Normal Equations. The nature of the weight matrices assumed and the structure of the design matrix on either side of the partition make it possible to simplify the equations (3-42) through (3-45) and (3-49) through (3-52) for computer coding so that this program could handle the data more efficiently and economically.

The partition of matrices enables the solution of the normal equation (3-42) to be sequential, i.e., to solve for V_{x1}, and then for V_{x2}. Equation (3-42) can be rewritten as

$$V_x = - N^{-1} U \tag{3-58}$$

with

$$N = \left(A^T P A + P_x \right) \tag{3-59}$$

and

$$U = A^T P W \tag{3-59}$$

Using the partition approach, the submatrices of N and U will be

$$N = \left[\begin{array}{c|c} N_{11} & N_{12} \\ \hline N_{21} & N_{22} \end{array}\right] = \left[\begin{array}{c|c} p A_1^T A_1 + p x_1 . I & p A_1^T \\ \hline p A_1 & (p + p x_2) . I \end{array}\right] \tag{3-60}$$

$$U = \left[\begin{array}{c} U_1 \\ \hline U_2 \end{array}\right] = \left[\begin{array}{c} p A_1^T W \\ \hline p W \end{array}\right] \tag{3-61}$$

Now, let

$$\left[\begin{array}{c|c} Q_{11} & Q_{12} \\ \hline Q_{12}^T & Q_{22} \end{array}\right] = \left[\begin{array}{c|c} N_{11} & N_{12} \\ \hline N_{12}^T & N_{22} \end{array}\right]^{-1} \tag{3-61a}$$

Then, from [Faddeev and Faddeeva, 1963]

$$Q_{11} = (N_{11} - N_{12} N_{22}^{-1} N_{12}^T)^{-1} \tag{3-62}$$

$$Q_{12} = - Q_{11} N_{12} N_{22}^{-1} \tag{3-63}$$

$$Q_{22} = N_{22}^{-1} (I - N_{12}^T Q_{12}) \tag{3-64}$$

and the solutions V_{x1} and V_{x2} are given by

$$V_{x1} = - Q_{11} \left[U_1 - N_{12} N_{22}^{-1} U_2\right] \tag{3-65}$$

$$V_{x2} = - N_{22}^{-1} N_{12}^T V_{x1} - N_{22}^{-1} U_2 \tag{3-66}$$

With the submatrices of N defined as in equation (3-60) in terms of the weight matrices and the design matrix A, it can be shown that

$$Q_{11} = \frac{p \cdot px_2}{p+px_2} \cdot A_1^T A_1 + px_1 \cdot I \tag{3-67}$$

It should be noted that since $A_1^T A_1$ is diagonal, Q_{11} is also diagonal.

$$\text{and } \bar{U} = U_1 - N_{12} N_{22}^{-1} U_2 = \frac{p \cdot px_2}{p+px_2} A_1^T W \tag{3-68}$$

Then, from equations (3-65) and (3-66)

$$V_{x1} = - Q_{11} \bar{U} \tag{3-69}$$

$$V_{x2} = - \frac{p}{p+px_2} \left[A_1 V_{x1} + W\right] \tag{3-70}$$

The weight coefficients matrix for the geoid undulations N (Ground Truth) is given by Q_{22} which is given by

$$Q_{22} = \frac{1}{p+px_2}\left[I + \frac{p^2}{p+px_2} A_1 Q_{11} A_1^T \right] \tag{3-71}$$

One of the advantageous features in this system is that both the matrices (Q_{11} and N_{22}) whose inverses are required are diagonal. This enables one to solve a system (of normal equations) of any size with relatively small computer storage requirement.

3.4.5.2 Constrained Solution. The solution of the normal equations for V_{x_1} and V_{x_2} will now be denoted by $V^*_{x_1}$ and $V^*_{x_2}$. With the notation for N^{-1} in equation (3-61a), equation (3-49) with equation (3-51) can be simplified as follows

$$CN^{-1}C^T = \begin{bmatrix} 0 & C_1 \end{bmatrix} \begin{bmatrix} Q_{11} & Q_{12} \\ Q_{12}^T & Q_{22} \end{bmatrix} \begin{bmatrix} 0 \\ C_1^T \end{bmatrix}$$

$$= C_1 Q_{22} C_1^T \tag{3-72}$$

$$W_c + CV_x^* = W_c + \begin{bmatrix} 0 & C_1 \end{bmatrix} \begin{bmatrix} V^*_{x_1} \\ V^*_{x_2} \end{bmatrix}$$

$$= W_c + C_1 V^*_{x_2} \tag{3-73}$$

Therefore,

$$\delta V_x = \begin{bmatrix} \delta V_{x_1} \\ \delta V_{x_2} \end{bmatrix} = - \begin{bmatrix} Q_{11} & Q_{12} \\ Q_{12}^T & Q_{22} \end{bmatrix} \begin{bmatrix} 0 \\ C_1^T \end{bmatrix} \left[C_1 Q_{22} C_1^T \right]^{-1} \left[W_c + C_1 V_{x_2}^* \right]$$

$$= \begin{bmatrix} Q_{12} C_1^T \\ Q_{22} C_1^T \end{bmatrix} \left[C_1 Q_{22} C_1^T \right]^{-1} \left[W_c + C_1 V_{x_2}^* \right] \qquad (3\text{-}74)$$

Then,

$$\delta V_{x_1} = - Q_{12} C_1^T \left(C_1 Q_{22} C_1^T \right)^{-1} \left(W_c + C_1 V_{x_2}^* \right) \qquad (3\text{-}75)$$

$$\delta V_{x_2} = - Q_{22} C_1^T \left(C_1 Q_{22} C_1^T \right)^{-1} \left(W_c + C_1 V_{x_2}^* \right) \qquad (3\text{-}76)$$

Once these correction terms are evaluated, the effective bias terms, V_{x_1}, are given by

$$V_{x_2} = V_{x_1}^* + \delta V_{x_1} \qquad (3\text{-}77)$$

Finally, the geoid undulations for any point on the profile is obtained by substituting the respective bias terms in equation (3-29a) as follows:

$$N = N_a^s - \Delta C_k \qquad (3\text{-}78)$$

This concludes the discussion on the mathematical formulation for analytical handling of the altimetry data.

PAGE INTENTIONALLY BLANK

4.0 ERROR ANALYSIS AND VALIDATION WITH PRELIMINARY DATA

4.1 Analysis and Evaluation of Preliminary Data

The analytical data handling formulations for this investigation called for the following basic inputs: (1) the altimeter ranges, and exact time (usually GMT) of each measurement to correlate it with (2) the associated orbit ephemeris, and (3) geoidal information used as geodetic control or benchmark along the subsatellite track to help define the geodetic scale of the outputs. The main outputs are: (1) the residual bias of the altimeter or calibration constant required to give a correct absolute geoidal scale, and (2) the geoidal profile, both deduced from the computer processing of the inputs using Least Squares processing with parameter weighting according to the aforementioned formulations.

Two sets of input data from Skylab mission SL/2, EREP pass #9, were used. Set A altimeter ranges have been corrected for all known sources of systematic errors including internal calibration constants, refraction and pulsewidth/bandwidth biases. Set B altimeter ranges were not corrected for these specific systematic errors. Figure 4-1 shows a sample of both sets of ranges. The objectives for processing these two sets were to investigate

(1) how well the modelling for systematic errors in the analytical data processing procedure can accomodate, recover and prevent such systematic errors from degrading the final results;

(2) the conditions required to optimally achieve the above objective.

Orbit A data were based on (a) reference ellipsoidal parameters a = 6378155 m and f = 1/298.255, (b) Smithsonian Astrophysical Observatory (SAO) 1969 Standard Earth Model with geopotential coefficients through degree 22 and order 16, (c) C-band and USB (Unified-S-band) radar tracking data, and (d) GM = 3.986013×10^{14} m^3/sec^2. Orbit B data were based on (a) a = 6378166 m and f = 1/298.3, (b) earth gravity model of 3 sectorial and tesseral terms, and 4 zonal terms, (c) C-band and USB radar tracking data, and (d) GM = 3.986032×10^{14} m^3/sec^2. Both orbits were corrected for other perturbation forces such as lunar gravitation, solar gravitation, earth tide, drag and solar radiation pressure. The geodetic datum for the tracking stations used in each orbit computation was assumed to be geocentric.

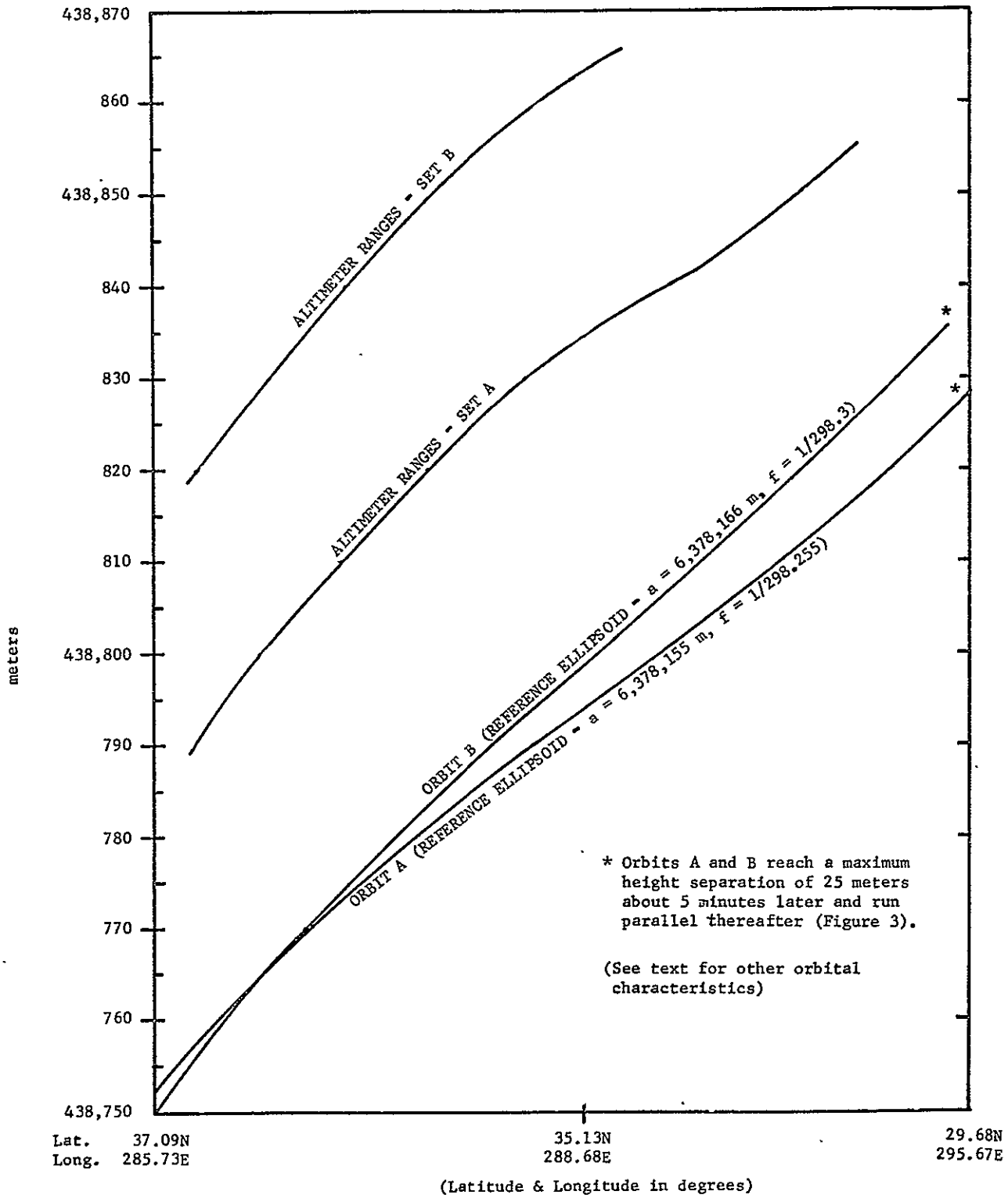

FIGURE 4-1. ALTIMETER RANGES (MODE 5) AND GEODETIC HEIGHT OF SKYLAB (SL-2 EREP PASS NO. 9) GMT 13:01:50 to 13:04:50

A segment of each of these two orbits is shown in Figures 4-1 and 4-2. Near to the U.S. east coast, (Figure 4-1), the two orbits are radially close but not parallel. Further away from the U.S. continent and tracking stations, the orbits diverge to a radial separation of about 25 meters and begin to run parallel (Figure 4-2). One or a combination of factors including the following may account for these deviations from theoretical expectancy

(1) Different gravitational constants (GM values) introduce different scales in the computed orbits.

(2) One or both of the two geodetic datums of the tracking stations may not be truly geocentric and free of rotational errors as assumed, or there may be undetected coordinates.

(3) The different gravity models influence the computed satellite ephemeris differently. However, the parallelism of the orbit segments away from continental tracking stations is either an accidental coincidence or a reflection that the geometrical constraints of the radar tracking data had ceased to be an influential factor.

(4) Differences in orbit computational techniques.

However, it is necessary to point out that by its configuration Skylab is not and was not designed to be a geodetic satellite with highest order tracking systems. Its mass is about 87440 kg. while the "effective" cross-sectional area employed in the orbit computations is 293.3m^2. In an absolute sense, the computed orbit may not be of geodetic quality. However, it is valid to assume that during short time intervals such as three minutes involved in the data sampling being analyzed, any systematic errors in the orbit will be constant in magnitude and sign. The analytical data processing procedure is designed to effectively accommodate this type of assumption. Therefore, precision wise, the altimeter data and the satellite ephemeris are consistent enough beyond expectations to warrant geodetic analysis.

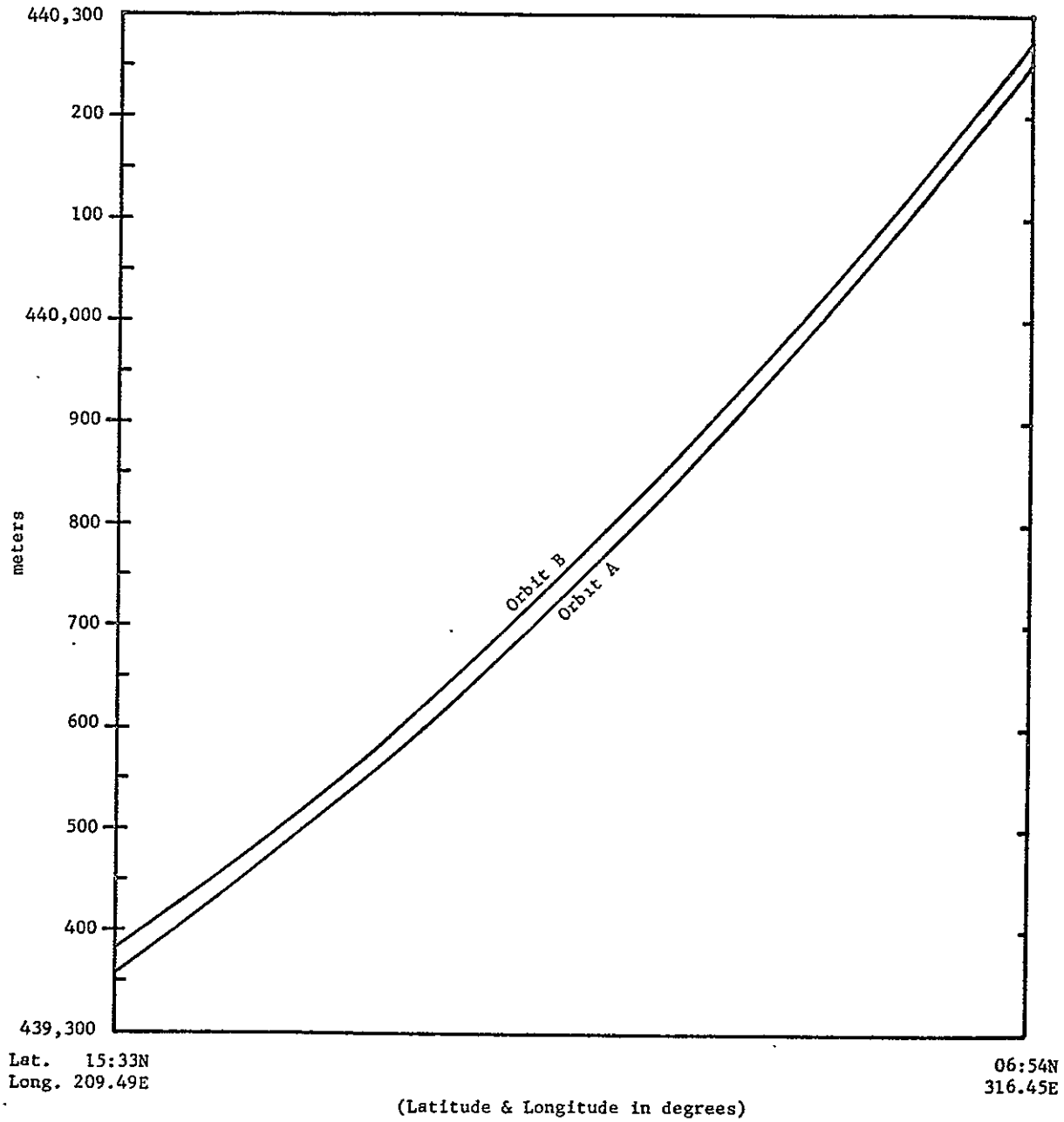

FIGURE 4-2. GEODETIC HEIGHT OF SKYLAB (SL-2 EREP PASS NO. 9)
GMT 13:10:00 to 13:13:00

The a priori geoid input was taken from Vincent and Marsh [1973] geoid. That geoid is not purely gravimetric as the name implies and therefore, in addition to a flattening of f = 1/298·255, a = 6378142m is also specified for its reference ellipsoid. To ensure compatibility of geodetic reference datums in equation (3-1), equation (3-10) was applied as necessary. The two sets of altimeter ranges and orbit ephemeris present four different data combinations that were processed. These various combination solutions were used in the analyses of (1) the efficiency of the data handling formulations, (2) the influences of orbit errors, and (3) the role of the choice of a priori geoidal ground truth. Some schools of thought believe that geoidal heights could be obtained by merely subtracting the altimeter ranges from the corresponding geodetic heights of the satellite. We computed and evaluated results from such a method which we consider invalid because it requires complete absence of systematic errors in the orbit and the altimeter which also must not drift, in order to ensure reliable results.

The Skylab altimeter data being used in the preliminary analysis were from mission SL-2, EREP pass #9 during which data were obtained in Modes 3 and 5 of the instrument's operation. For this pass, the signal to noise ratio appeared to be relatively low during Mode 3. Therefore, only the Mode 5 data were used.

4.2 Results and Analysis

From the given satellite orbit and measured altimeter ranges, the overall objective of the investigation is to simultaneously (a) determine a geodetic calibration constsnt(s) that (b) corrects or adjusts the altimeter ranges for (c) determination of absolute geoidal heights with correct scale. Tables 4-1 to 4-3 and Figures 4-1 and 4-2 show the geodetic heights of the orbits and the altimeter ranges designated as Set A and Set B as previously described. All the results being analyzed have been modified to be based on a reference ellipsoid of a = 6,378,142 m. and f = 1/298·255.

TABLE 4-1. GEODETIC HEIGHT OF SKYLAB AND A PRIORI GEOIDAL HEIGHTS INVOLVED IN DATA ANALYSIS
(Values are in meters and modified to refer to an ellipsoid a = 6378142m, f = 1/298·255)

Skylab Geodetic Heights Based on		A Priori Geoidal Height Input
Orbit A	Orbit B	
438769.7	438780.5	-41.7
438770.2	438781.2	-41.8
438770.8	438781.8	-42.0
438772.5	438783.4	-42.4
438773.6	438784.8	-42.7
438775.2	438786.7	-43.1
438776.8	438788.6	-43.5
438778.3	438790.4	-43.9
438779.8	438791.8	-44.3
438781.8	438793.7	-44.8
438782.7	438795.3	-45.2
438783.2	438795.9	-45.3
438783.7	438796.4	-45.5
438785.1	438798.1	-45.8
438786.0	438799.0	-46.2
438787.4	438800.6	-46.6
438788.2	438801.6	-46.9
438788.7	438802.1	-47.0
438789.1	438802.7	-47.1
438790.4	438804.5	-47.5
438791.3	438805.5	-47.8
438792.5	438806.7	-48.3
438793.8	438808.2	-48.7
438794.2	438808.9	-48.8
438794.6	438809.4	-49.0
438795.8	438810.6	-49.0
438796.6	438811.7	-49.0
438797.8	438813.0	-49.1
438798.6	438813.8	-49.2
438799.0	438814.3	-49.3
438799.4	438814.8	-49.3
438800.5	438816.3	-49.4
438801.3	438817.2	-49.5
438802.5	438818.4	-49.7
438803.6	438819.9	-49.8
438804.8	438820.3	-50.0
438804.3	438820.7	-49.9
438806.2	438822.8	-49.7
438807.0	438823.8	-49.7
438808.1	438825.3	-49.6
438808.5	438825.6	-49.5
438808.8	438826.0	-49.5
438810.0	438827.4	-49.5

TABLE 4-2. ANALYTICALLY ADJUSTED RANGES
EREP PASS 9 OF SL-2
(values in meters)

GMT 13:01:57·981 to 13:02:52·062

Measured Altimeter Ranges		Based on Orbit A Adjusted Altimeter Ranges		Based on Orbit B Adjusted Altimeter Ranges	
SET A	SET B	SET A	SET B	SET A	SET B
438789.1	438818.6	438811.9	438811.9	438824.6	438824.7
438788.7	438819.3	438811.5	438812.6	438824.2	438825.3
438791.0	438819.8	438813.8	438813.2	438826.5	438825.9
438790.6	438821.8	438813.4	438815.2	438826.1	438827.9
438796.2	438823.4	438819.0	438816.7	438831.7	438829.4
438797.0	438825.9	438819.8	438819.3	438832.5	438832.0
438797.7	438827.7	438820.5	438821.0	438833.2	438833.8
438799.6	438829.2	438822.4	438822.5	438835.1	438835.2
438801.1	438831.4	438823.9	438824.8	438836.6	438837.5
438803.3	438832.7	438826.1	438826.0	438838.8	438838.7
438806.3	438835.1	438829.1	438828.5	438841.8	438841.3
438806.3	438835.6	438829.1	438829.0	438841.8	438841.7
438806.3	438836.2	438829.1	438829.6	438841.8	438842.3
438808.2	438837.8	438831.0	438831.1	438843.7	438843.9
438809.3	438838.8	438832.1	438832.2	438844.8	438844.9
438810.8	438840.4	438833.6	438833.8	438846.3	438846.5
438811.2	438840.8	438834.0	438834.2	438846.7	438846.9
438813.1	438841.6	438835.9	438834.9	438848.6	438847.6
438813.5	438842.0	438836.3	438835.4	438849.0	438848.1
438814.2	438844.4	438837.0	438837.7	438849.7	438850.4
438815.7	438845.6	438838.5	438838.9	438851.2	438851.6
438817.2	438846.4	438840.0	438838.8	438852.7	438852.5
438818.7	438848.5	438841.5	438841.8	438854.2	438854.6
438820.2	438849.1	438843.0	438842.5	438855.7	438855.2
438820.6	438849.4	438843.4	438842.8	438856.1	438855.5
		Geodetic Calibration Constant			
		22·8	-6·6	35·5	6·1

TABLE 4-3. ANALYTICALLY ADJUSTED RANGES
EREP PASS 9 OF SL-2
(values in meters)

GMT 13:02:38.542 to 13:03:33.661

Measured Altimeter Ranges		Based on Orbit A Adjusted Altimeter Ranges		Based on Orbit B Adjusted Altimeter Ranges	
SET A	SET B	SET A	SET B	SET A	SET B
438813.5	438842.0	438836.7	438835.9	438852.3	438851.5
438814.2	438844.4	438837.4	438838.3	438853.0	438853.8
438815.7	438845.6	438838.9	438839.4	438854.5	438855.0
438817.2	438846.4	438840.4	438840.3	438856.0	438855.9
438818.7	438848.5	438841.9	438842.4	438857.5	438857.9
438820.2	438849.1	438843.4	438843.0	438859.0	438858.5
438820.6	438849.4	438843.8	438843.3	438859.4	438858.9
438821.0	438851.3	438844.2	438845.2	438859.8	438860.7
438822.8	438851.8	438846.0	438845.7	438861.6	438861.3
438824.0	438853.2	438847.2	438847.1	438862.8	438862.6
438824.3	438854.3	438847.5	438848.2	438863.1	438863.8
438825.5	438855.1	438848.7	438848.9	438864.3	438864.5
438825.5	438854.6	438848.7	438848.4	438864.3	438864.0
438826.2	438855.7	438849.4	438849.5	438865.0	438865.1
438827.3	438856.8	438850.5	438850.7	438866.1	438866.3
438828.1	438857.9	438851.3	438851.8	438866.9	438867.3
438829.2	438859.7	438852.4	438853.6	438868.0	438869.2
438831.5	438859.9	438854.7	438853.8	438870.3	438869.4
438831.8	438860.3	438855.0	438854.2	438870.6	438869.8
438833.7	438861.9	438856.9	438855.8	438872.5	438871.3
438832.6	438862.7	438855.8	438856.6	438871.4	438872.2
438835.6	438864.4	438858.8	438858.3	438874.4	438873.9
438835.2	438864.6	438858.4	438858.5	438874.0	438874.0
438834.5	438864.1	438857.7	438858.0	438873.3	438873.6
438837.1	438865.7	438860.3	438859.6	438875.9	438875.2
		Geodetic Calibration Constant			
		23.2	-6.1	38.8	9.4

4.2.1 Calibration Constants and Adjusted Altimeter Ranges

As developed earlier, the altimeter bias, radial errors in orbit determination, and errors from inadequate or total lack of correction for significant sea state variations are all algebraically additive. These errors are inseparable unless two of them are absolutely known. In this investigation, the total sum of all three is the geodetic calibration constant to be determined.

Unfortunately, unless the radial orbit error is zero, some known absolute geoidal height must be used as geodetic control or benchmark in order to determine the required geodetic calibration constant. In this case, the calibration constant so determined is scalewise-dependent on the geodetic datum of the a priori geoidal input or the geodetic control used. This is demonstrated in Figure 4-3. In Figure 4-3, GG-73 is the subsatellite geoid segment taken from Vincent and Marsh [1973] geoid. AA is the resultant satellite altimetry geoid segment based on GG-73 as a priori input. This a priori input and its output are used as a yardstick or control of the experiment to investigate the effects of errors in a priori geoid height inputs and scale dependency of the computed geodetic calibration constant and satellite altimetry geoid heights on geodetic control (ground truth). Errors were introduced into GG-73 to produce A-I. The resultant satellite altimetry geoid segment from using A-I as a priori input is A-O. Similarly, B-O results from the use of B-I as a priori input.

It is obvious that AA (the control experiment) is shape-wise identical to A-O and B-O. For each case, normalized parameter weighting, consistent with the estimated absolute accuracy of the a priori geoidal height input, was applied. In all cases, even though the resultant point to point geoidal height differences were exactly identical, the deduced calibration constants and hence the values of the computed geoid heights depended on the weighted a priori geoidal height inputs. Figure 4-3 definitely shows that such a priori inputs and the errors in them affect only the linear scale of the calibration constant and not the shape of the deduced geoid from the type of analytical processing used herein. In other words, the main effect of the a priori geoid input is reflected in the position of the computed geoid relative to geocenter. To determine the geoid with correct shape and scale and centered at geocenter (i.e., an absolute geoid) is the ultimate objective of all geoid computations, and the criteria for the geoid to contribute to solutions of problems in oceanography, geophysics, geodesy and the earth's gravity field model.

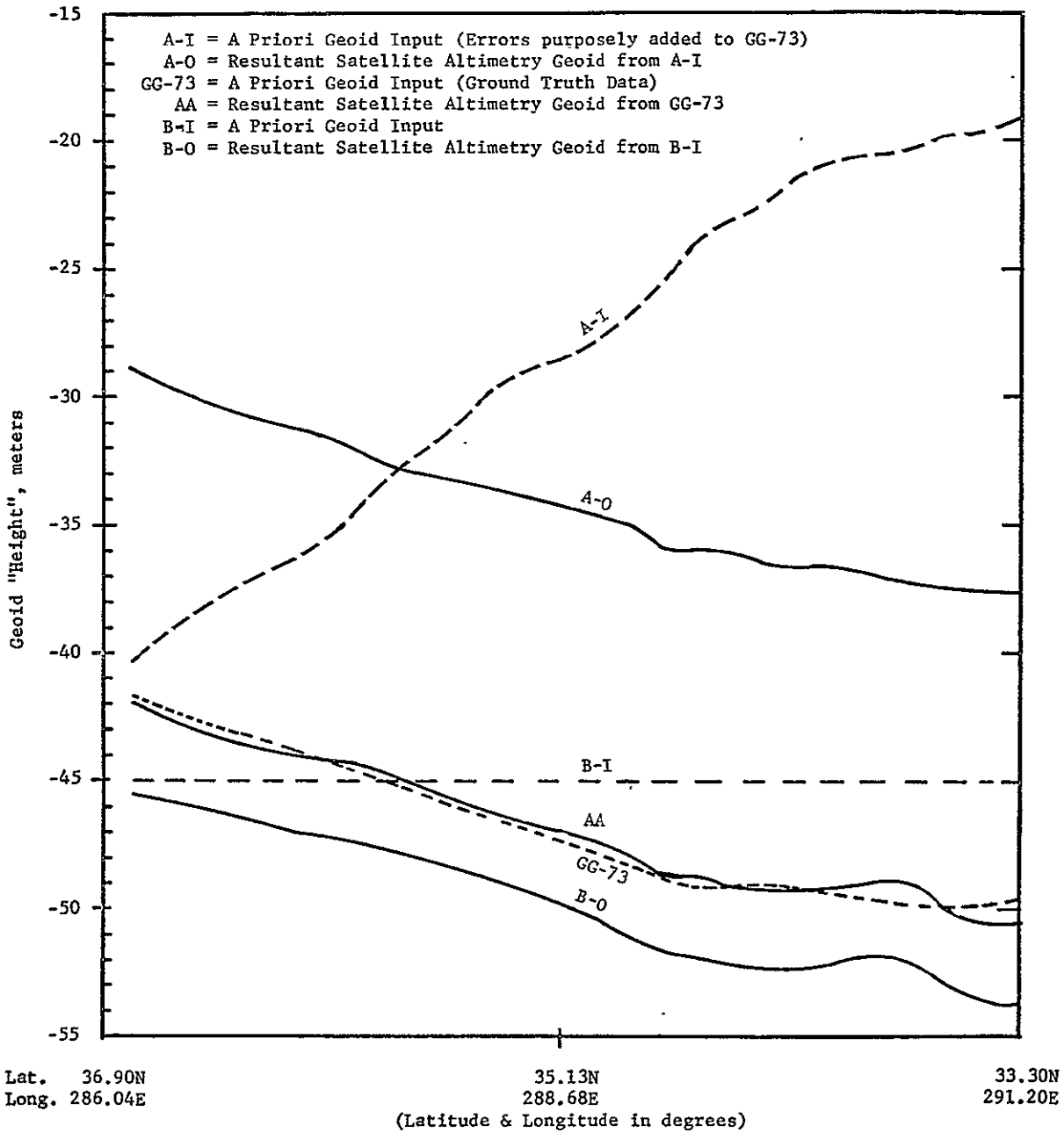

FIGURE 4-3. EFFECT OF ERRORS IN A PRIORI GEOID HEIGHT INPUTS AND SCALE DEPENDENCY OF CALIBRATION CONSTANT AND GEOIDAL HEIGHT ON GEODETIC CONTROL (GROUND TRUTH)

In the Skylab data, the altimeter bias appears to vary with the modes and the sub-modes which are described in Kern and Katucki [1973]. This was another factor taken into account. For the current data processing, the additional assumption is that for a "short time interval", the systematic radial orbital errors are of constant magnitude and sign. These two factors constrain the current "short time interval" for this set of data to be no more than 3 minutes. From the calibration constants shown in Tables 4-2 and 4-3 the assumption of constant radial orbital errors is better satisfied by Orbit A than Orbit B. For Orbit A, the rate of change in radial errors during this period (close to tracking station) is about 0·5 m per 2 minutes, for Orbit B it is about 3 m per 2 minutes of time. There are currently some avoidable errors in the computation of Orbit B as shown in Wollenhaupt and Schiesser [1973]. In particular the gravity model can be improved. This result supports a well known fact that the earth gravity model required for accurate orbit computation is a very important factor.

A key indicator of the reliability of the analytically computed geodetic calibration constant is the consistency of the adjusted ranges. The mathematical model developed for this analysis anticipated imperfections in the knowledge of (1) the orbit and (2) the delay constants (biases) for transforming the radar altimeter returns into ranges in engineering units for geodesy. These problems algebraically add up to be a linear radial error relative to the earth's geocenter. Through the use of the discussed appropriately weighted a priori geoidal heights; (a) no matter what the errors in the different sets of ranges used, the derived adjusted ranges should be identical if the same orbit is used; (b) alternatively, if a unique set of ranges is used with different orbit data, the adjusted set of ranges should differ by only the radial differences between the orbits. The expectations (a) and (b) are established to within the noise level of the data by the results of Tables 4-2 and 4-3. Conversely, the deduced geodetic calibration constants should also satisfy condition (b). Thus from Table 4-2, the constants 22·8 minus 35·5 should equal -6·6 minus 6·1, and from Table 4-3, 23·2 minus 38·8 should equal -6·1 minus 9·4, meters.

4.2.2 Geoidal Heights Analytically Deduced from Satellite Altimetry

Figure 4-4 shows the deduced geoidal heights from the analytical processing of the four data combinations already described. Figure 4-4 also shows three other profiles for the same segment of the geoid as given by Vincent, et al [1972 and 1973] using different conventional techniques. As usual, (see Fubara and Mourad [1972] and Fischer, et al [1968]) these other conventional geoid profiles disagree with each other significantly. In Figure 4-4, GG-72 and GG-73 are conventional geoid segments primarily based on global gravity data which are too sparse and often very inaccurate in ocean areas (70% of the globe) and therefore satellite-derived geopotential coefficients were used to augment the measured gravity data. The present day accuracy and extent of coverage of global gravity data and the geoid are discussed in Decker [1972], and Fubara and Mourad [1973].

By using Orbit A, remarkable agreement achieved (Figure 4-4) between the analytically computed satellite altimetry geoid segments AA, and AB and GG-73, the Vincent and Marsh [1973] geoid is beyond all expectations. It implies that in the area of the investigation either the GG-73 geoid and Skylab altimeter are extremely accurate or that certain factors have cancelled out to produce such a sub-meter agreement. As has been shown and well accommodated by our analytical data handling model, it is logical to assume that whatever systematic radial errors exist in the computed orbits for the short time period involved, such errors should be constant in magnitude and sign. It is therefore valid to assume that, provided the altimeter system is stable, the deduced altimeter geoid should very closely approximate the true geoid shape of that segment. However, the "absoluteness" scalewise and in orientation of the geoid height is dependent on the orbit and/or the geodetic control that should be used. Such a valid geodetic control or benchmark was not available for this investigation.

The results from using Orbit B shown as segments BB and BA of Figure 4-4, show a systematic tilt relative to GG-73 and the results based on Orbit A. The main differences between Orbit A and B have been discussed earlier. The conclusion is that the geodetic outcome of satellite altimetry is extremely sensitive to the computed orbit. The agreement between segments AA and AB based on the same orbit but different sets of ranges, one of which set has known systematic errors, shows that our analytical basis is valid and workable for recovery and elimination of the influences of such systematic errors. The same matching applies to BB and BA.

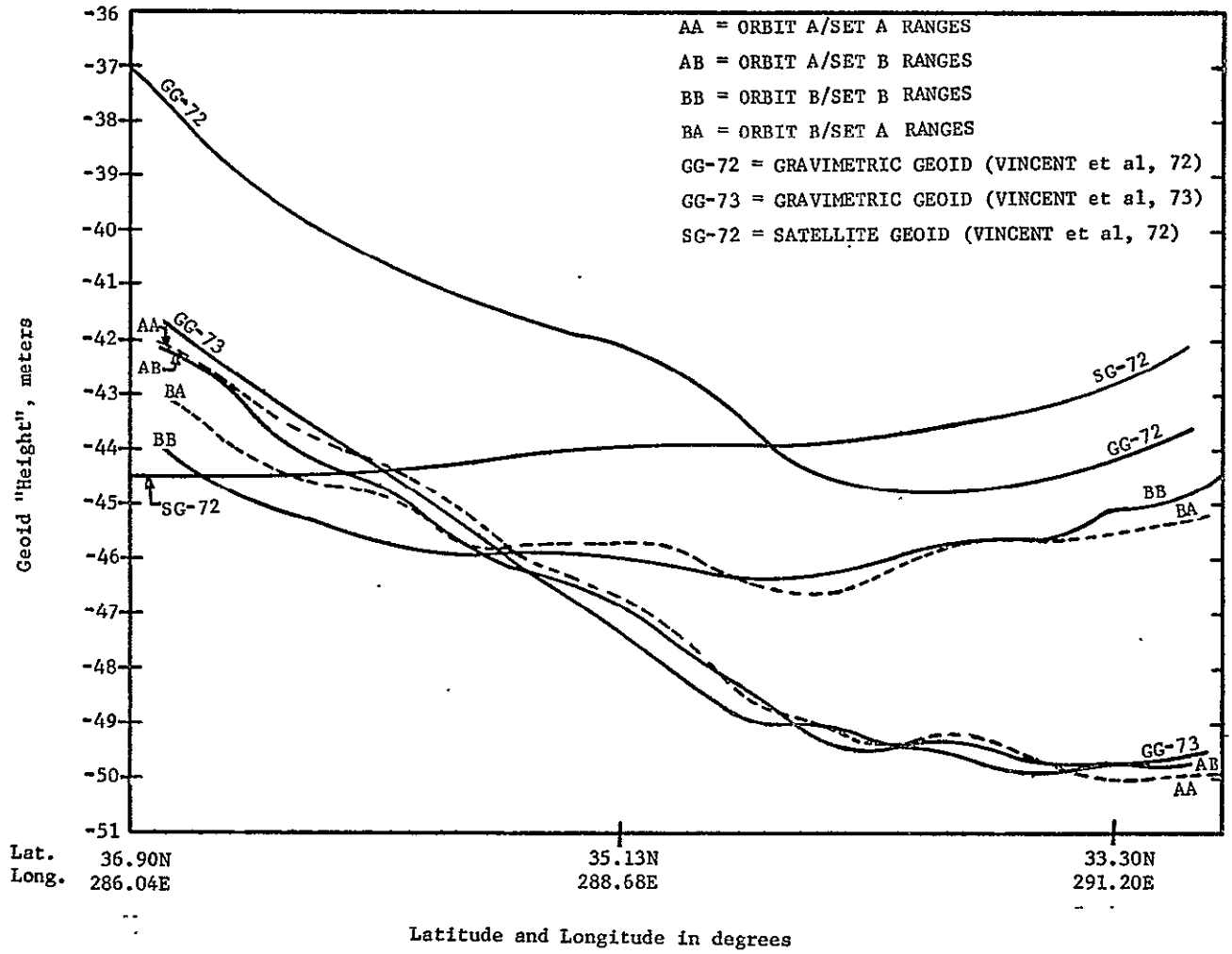

FIGURE 4-4. CONVENTIONAL GEOID AND SATELLITE ALTIMETRY GEOID SEGMENTS (SKYLAB SL-2 EREP PASS 9 DATA)

By merely subtracting the measured altimeter ranges from the corresponding satellite geodetic heights, the resultant profiles for the four data combinations are shown in Figure 4-5. Compared to the results in Figure 4-4, the simple subtraction results of Figure 4-5 show, for the Orbit A, remarkable contrast between the "geoid" AA (-19 m to -27•5 m) and AB (-49 m. to -56 m.); for Orbit B and the same two sets of altimeter ranges, "geoid" BB (-38 m. to -40 m. to -39 m.) differ from BA (-8 m. to -11 m. to -10m.). Thus this simple subtraction approach is sensitive not only to the orbit but also to the systematic errors in altimeter ranges unlike the analytical approach. The remarkable match between the analytically computed geoid segments from EREP pass #9, mode 5 data, and Orbit A as given in Figure 4-4 and the corresponding conventional geoid profile from Vincent and Marsh [1973], as deduced from a combination of terrestrial gravity measurements and satellite-derived geopotential coefficients, should be accepted with caution. Precision estimate of this conventional geoid is about $\pm$ 5 to $\pm$ 15 meters in ocean areas, according to the authors. However, from Rapp [1973], this estimate may be optimistic, in view of certain error sources not accounted for in the computation of that conventional geoid. Furthermore, the segment of the conventional geoid plotted, was scaled off a very small scale world map. This latter process would normally introduce errors into the plotted segment. This condition easily introduces systematic displacement errors which are not conducive to reliable comparison between the two types of geoid segments.

In spite of all these possible sources of discrepancy, and the data errors and uncertainties previously outlined, the comparison of features between the altimetry geoid and this particular conventional geoid (no two conventional geoids are alike and often differ by tens of meters and relative tilts) is very encouraging. These preliminary results have not been corrected for the influences of sea state, possible nadir alignment errors and departures of the sensor field of view from the nadir. Some of the high frequency features of the satellite altimetry geoid which may be a reflection of these uncorrected influences have been smoothed out. The altimeter ranges refer to some mean sea surface topography of the instant of measurement called MISS in Figure 1-1. The quasi-stationary departures of the MISS from the geoid is significant in the area of this

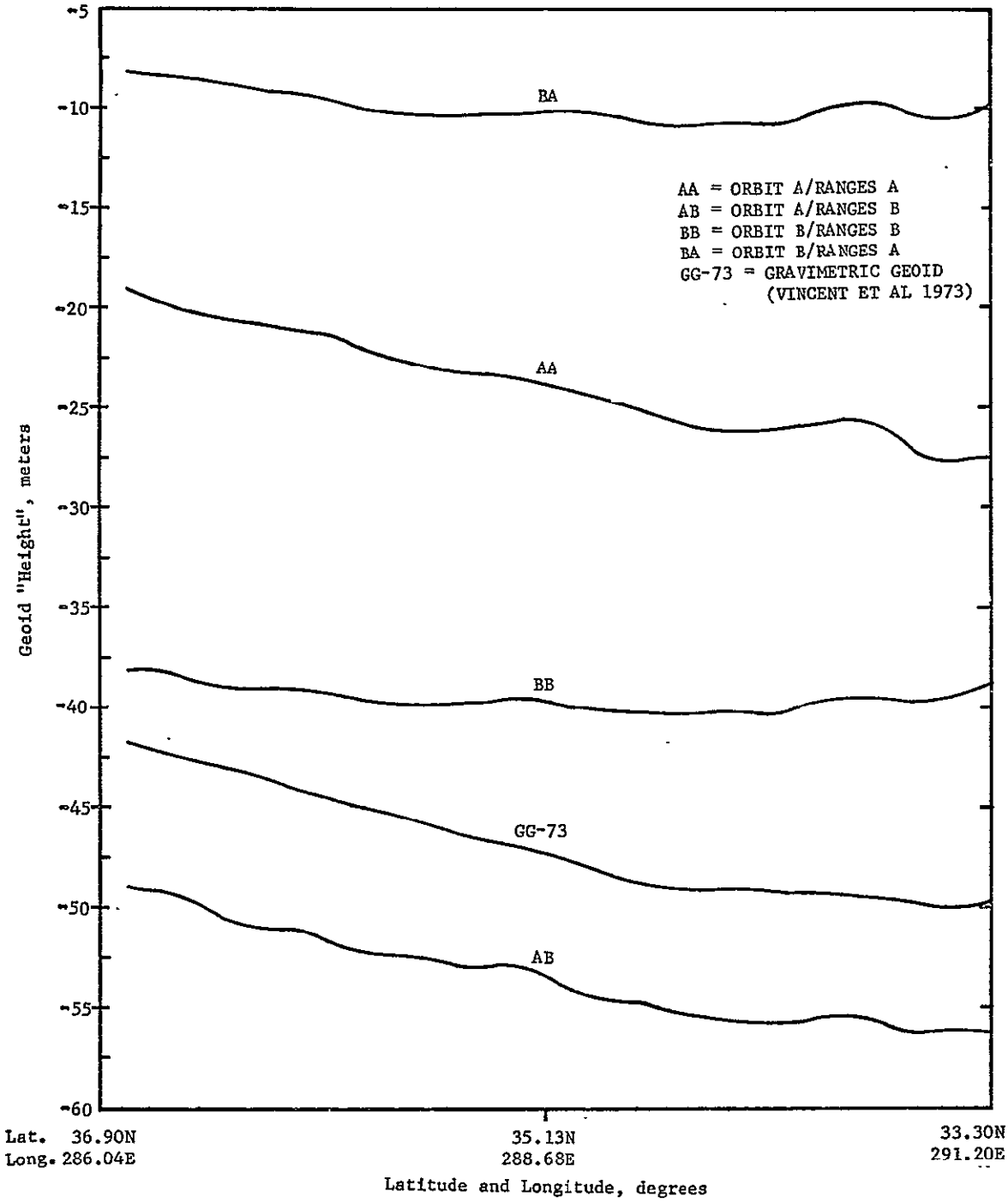

FIGURE 4-5. SATELLITE HEIGHT MINUS ALTIMETER RANGES AND A CONVENTIONAL GEOID PROFILE (SKYLAB SL-2 EREP PASS 9, MODE 5 DATA)

investigation according to Figures 1 and 2 of Sturges [1972]. If the altimeter is as precise as these results indicate, the expected trend in average sea surface topography of the area could have been sensed.

4.3 Conclusions From the Preliminary Analysis

The preliminary conclusions from these quick-look data investigations and previous simulation studies include:

(1) The analytical data handling formulations developed for this investigation appear to be very satisfactory. The main outputs required, the geodetic calibration constant, the geoid height and the corrected altimeter ranges were reliably determined.

(2) To ensure that the deduced calibration constant and geodetic heights are absolute, the use of geodetic control or a benchmark whose absolute geoidal height is known is indispensable. The establishment of such controls from a combination of astrogravimetry and satellite data is discussed in Mourad and Fubara [1972b], and in Fubara and Mourad [1972a] and the practical implementation is partially demonstrated in Fubara and Mourad [1972b]. There is an implicit correlation between this conclusion and the conclusion based on a different type of investigation in Rapp [1971] that: "In carrying out simulation studies with non-global data it was concluded that altimetry data could not be used alone for potential coefficient determination.... Consequently, the altimetry data was combined with geoid undulation information in non-ocean blocks and with existing terrestrial gravity data.".

(3) On the assumption that the altimeter system is stable, and that systematic orbit radial errors for short time periods are constant, the altimeter geoid shows very high frequency details which have been smoothed out in the plotted geoid or more accurately the sea surface topography. Such high frequency details may also reflect the inexact fulfillment of various assumptions implied or the uncorrected influence of sea state.

(4) These preliminary results indicate that satellite altimetry will be a valid and useful tool for computing quasi-stationary departures of sea surface topography from the geoid. This practical application is important to oceanographic work related to ocean dynamic phenomena such as circulation patterns, water mass transport, ocean tides, ocean current influences, etc. These in turn relate to air-sea interaction and the knowledge for global numerical weather prediction. Such oceanographic factors also affect our knowledge of pollution dispersion by the oceans, an important guiding factor in waste disposal, and prediction of dispersal and control of oil spill hazards. Further developments on these issues are in Fubara and Mourad [1973].

(5) Orbit computation in which inadequately calibrated altimeter ranges are employed as constraints is not desirable and present no advantage for processing altimeter data to compute the geoid. First, the unmodelled range biases introduce large systematic errors that are not admissible in least squares orbit computation. Such systematic errors cannot be accurately eliminated through modeling unless some valid geodetic controls are used as constraints. Second, the use of orbits computed in this way to deduce a geoid from the same altimeter data with purely differencing or graphical techniques would be misleading. For example, the geoid so deduced would closely match the original geoid used in applying the altimeter ranges as a constraint in the orbit computation.

(6) Deduction of a correctly scaled geoid from satellite altimetry cannot be achieved by merely subtracting altimeter ranges from the corresponding geodetic heights of the satellite unless (a) the satellite orbit is errorless, (b) the altimeter does not drift, and (c) the altimeter system biases are either non-existent or are absolutely known. Therefore, in practice, at this time, satellite altimetry ranges cannot be regarded as representing direct determination of absolute geoid heights as one would like to assume. At this time marine geodesy, involving the use of astrogravimetric and satellite geodesy techniques, appears indispensable for the provision of geodetic controls required for the full achievement of satellite altimetry objectives of GEOS-3, and SEASAT series of the NASA "Earth and Ocean Physics Applications Program".

5.0 PROCESSING OF THE ALTIMETRY DATA FROM EREP PASSES #4, #6, #7, and #9

5.1 Evaluation of the Input Data

The analysis of the altimetry data was made only for EREP passes #4, #6, #7, and #9 whose approximate locations in the North Atlantic Ocean are shown in Figure 5-1. The analysis was accomplished in three basic steps: (1) Filtering, (2) Estimation of the parameters, and (3) Graphical presentation of the results. The basic inputs for the first step are (a) the altimeter ranges and the exact time of each measurement to correlate it with, (b) the associated orbit ephemeris, (c) the parameters of the reference ellipsoid, and (d) the covariance funtion for the geoid undulations.

The satellite altimetry data for the four passes were received on magnetic tapes from NASA/JSC. These data consist of eight altimeter range observations in frames at 1.04 seconds interval. However, for the purpose of this investigation, the mean of the eight observations in each frame is considered as one observation. This assumption should not deteriorate the results for the following reasons: A frame of observations covers an effective area of about 6 km by 13 km, since the ground speed of the Skylab was about 7 km/sec and the radius of the radar foot print was about 3 km [McGoogan, et al, 1974]. Considering the accuracy of the altimeter system on board the Skylab, the change in geoid over an area of size 6 km by 13 km would be insignificant. Each frame has eight observations made at equal intervals. The Skylab Best Estimate Trajectory (Skybet) data are also available on a tape at intervals of exactly 1/8 of a second. Only the earth fixed geocentric coordinates of the Skylab and the time of observation are input from these data.

The best available estimates for the shape and size of the geodetic reference ellipsoid are given by

flattening = 1/298.255

Semi major axis diameter = 6,378,142.0 meters

Incidentally, this is the same as the reference ellipsoid to which the Marsh-Vincent 1973 geoid is referred. The covariance function for geoid undulation is taken from Tscherning and Rapp [1974]. This is a numerical covariance

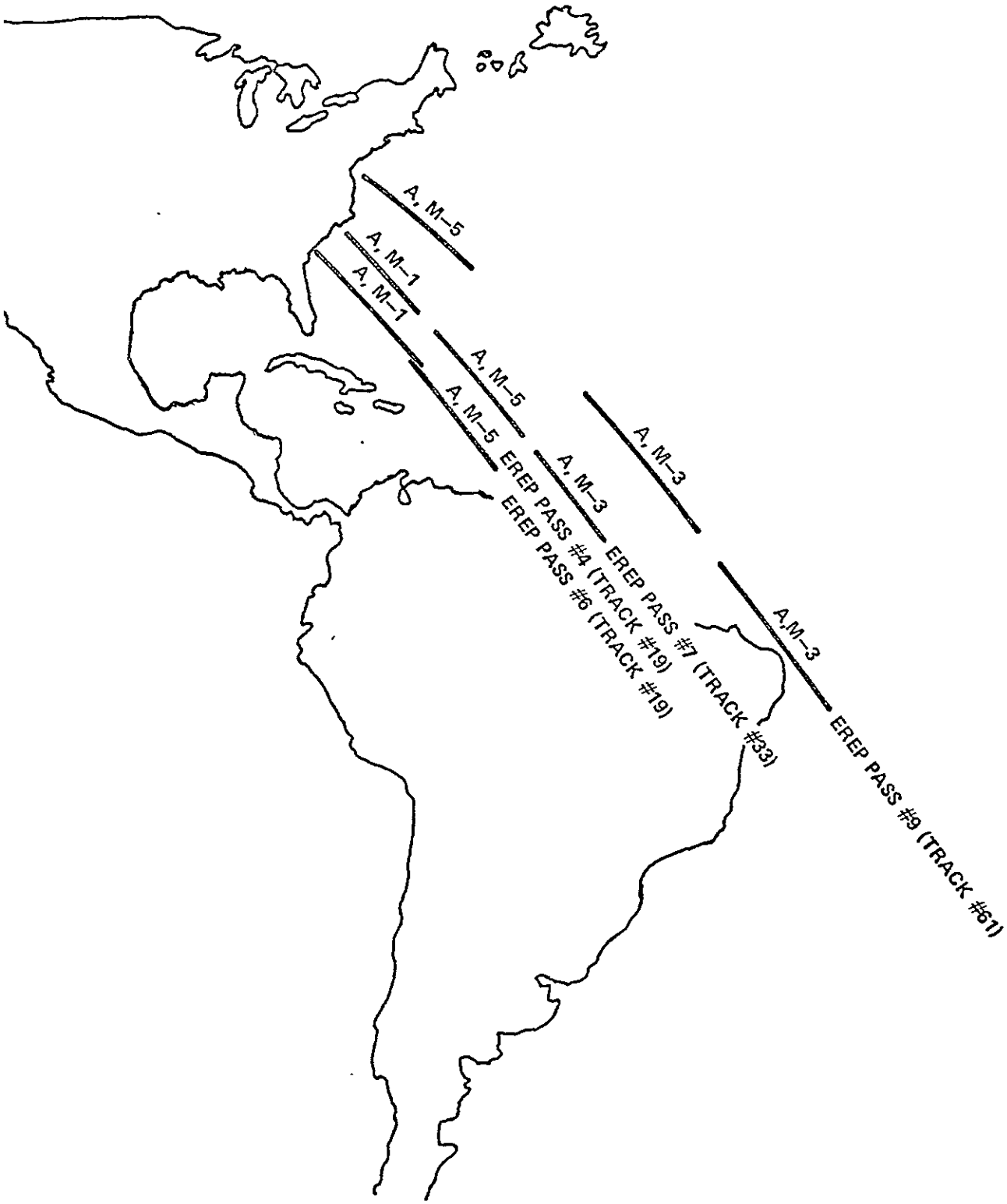

FIGURE 5-1. S193 - SKYLAB SL-2 ALTIMETER DATA,
PASSES 4, 6, 7 & 9, MODES 1, 3, AND 5

function compatible with the reference ellipsoid chosen for the analysis. Some values of this covariance function are presented in Table 5-1, along with the corresponding spherical arc distances. For any spherical distance, other than the tabulated points, the covariance function is obtained by linear interpolation.

The output from the filtering step is a set,each of filtered and unfiltered residual altitude, which is the difference between the height of the satellite above the reference ellipsoid and the altimeter ranges. A set of geodetic latitudes and longitudes of the subsatellite points at the times of the altimeter observations, is also a part of the output from this step.

The residual altitudes which are filtered in the first step and the ground truth geoid undulations taken from the Marsh-Vincent geoid map [1973] form the input for the second step which is the estimation of the calibration constants and the geoidal parameters. In the third step, the estimated geoid profiles are plotted against time along with the ground truth profiles for easy comparison for shape.

The altimetry data in each pass were observed in several submodes each of which consists of several sub-submodes of observations. The altitude measurement of the satellite above the ocean which is the only geodetic data of interest, comes only from Modes 1, 3, and 5 of the Skylab altimeter [McGoogan, et al, 1974]. The residual altitude which is the difference between the height of the satellite above the reference ellipsoid and that above the ocean surface is a measure of the geoid undulation at the nadir point of the satellite [Gopalapillai, 1974]. The maximum magnitude of the geoid undulations, referred to the best available reference ellipsoid, is of the order of about 125-150 meters. Therefore, any residual altitude of more than a conservative estimate of 300 meters, is an indication of instrument malfunction in the altimeter measuring system. Consequently, data processing was done only for those segments of the passes (#4, #6, #7, and #9) corresponding to modes 1, 3, or 5 where the absolute residual altitude is less than 300 meters. The various segments of the altimetry data and their suitability for geodetic processing are presented in Table 5-2 where the segments are identified by time intervals.

TABLE 5-1. COVARIANCE FUNCTION (NUMERICAL) FOR GEOID UNDULATIONS

Spherical Distance(ψ)	Covariance Function(m^2)
0.0	926.1
0.5	925.0
1.0	922.4
1.5	918.8
2.0	914.3
2.5	909.1
3.0	903.3
3.5	896.9
4.0	890.0
5.0	874.9
6.0	858.2
8.0	820.7
10.0	778,9
12.0	733.7
14.0	685.9
16.0	636.0
18.0	584.8
20.0	532.7
22.0	480.2
24.0	427.7
26.0	375.7
28.0	324.5
30.0	274.4
35.0	156.2
40.0	50.9
45.0	-38.7
50.0	-110.8

It appears that the data from different submodes are associated with distinctly different bias terms. Therefore, the submodes in each pass are sequentially numbered for convenience of handling the data and these numbers are referred to as submodes* in the rest of this report. Examination of Table 5-2 reveals that the processable (good) data come from submodes 0, 1, and 2 in Mode 1 and 5 and from submodes 3, 4, and 5 in Mode 3.

It is assumed that the necessary corrections for errors caused by internal delay, switching pulse widths and band widths, and pointing within certain modes and submodes and by tropospheric refraction, have already been made. Any residual systematic errors will be absorbed in the bias terms recovered in this analysis especially when an independent bias term is considered to be associated with each submode. Even the errors due to the uncertainties in the orbit and to the off nadir pointing can be filtered out this way if they are constant over the short segments of the passes considered.

5.2 Procedure

5.2.1 Filtering

The equations required for the filtering process have been presented in chapter 3.0. These equations are repeated here for easy reference.

$$N_a^s = C_{ss}\bar{C}^{-1}N_a \tag{3-31}$$

with

$$\bar{C} = C_{ss} + C_{nn} \tag{3-31a}$$

where,

$$C_{nn} = \sigma^2 I \tag{3-32}$$

TABLE 5-2. VARIOUS SEGMENTS OF THE ALTIMETRY DATA PROFILES

Pass	Mode	Date	Submode	Submodes* (# Assigned)	Time From	Time To	Suitability of Data for Geodetic Processing
4	1	155	0,1,2	1,2,3	17 11 11·335	17 14 3·976	Suitable
			3,4,5	4,5,6	14 6·056	14 23·736	Unsuitable
	5		0,1	7,8	15 16·799	16 36·879	Suitable
6	5	160	0,1,2	1,2,3	15 15 31·400	15 18 21.960	Suitable
			3,4,5	4,5,6	18 24·040	18 41·720	Unsuitable
7	1	161	0,1,2	1,2,3	14 28 12·809	14 31 05·449	Suitable
			3,4,5	4,5,6	31 7·529	31 25·209	Unsuitable
	5		0,1,2	7,8,9	32 10·406	34 51·605	Suitable
			3,4,5	10,11,12	34 53·685	35 28·193	Unsuitable
	3		0,1,2	13,14,15	35 32·360	36 19·160	Unsuitable
			3,4,5	16,17,18	36 26·440	38 45·800	Suitable
9	5	163	0,1,2	1,2,3	13 1 36·142	13 4 26·701	Suitable
			3,4,5	4,5,6	4 28·781	4 46·461	Unsuitable
			0,1,2	7,8,9	9 2·170	9 48·969	Unsuitable
			3,4,5	10,11,12	10 0·410	12 20·809	Suitable
			6,7,0, 1,2	13,14,15, 16,17	12 23·928	15 31·086	Unsuitable
			3,4,5	18,19,20	15 35·246	17 55·646	Suitable
			6,7	21,22	17 58·766	18 42·445	Unsuitable

These computations include the inversion of a symmetric matrix $\bar{C}$ of size equal to the number of observations included in the filtering. In order to avoid inverting very large matrices, only those observations which belong to the same submode* from each pass have been included for simultaneous filtering. This limited the maximum number of observations in any one attempt to about 100 in the data processed in this investigation.

The elements c_{ij} of the C_{ss} matrix corresponds to the auto-covariance given in Table 5-1 corresponding to the spherical distance, ψ between the i^{th} and j^{th} observations. On the profile under consideration, ψ is given by

$$\text{Cos } \psi = \sin\varphi_i \sin\varphi_j + \cos\varphi_i \cos\varphi_j \cos\Delta\lambda_{ij} \tag{5-1}$$

where φ_i and φ_j are the lattitudes of the observations i and j and $\Delta\lambda_{ij}$ is the difference in longitude between these two observations. Incidentally the latitudes of the observations are obtained in an iterative solution from the earth-fixed geocentric coordinates of the satellite positions (at the time of observations) using equations (3-6) and (3-7). The longitudes, λ, are computed using the following equation:

$$\tan\lambda = \frac{Y_s}{X_s} \tag{5-2}$$

The only other quantity which needs to be defined before proceeding with the computations, is σ. A nominal value of one meter which is considered realistic for the Skylab altimeter, is assumed. However, for pass #7 where the signal to noise ratio is very low, both one and two meters were used.

The instructions detailed in this procedure have been coded in a Fortran IV computer program which punches out both the input altimeter data and the filtered signal along with the latitude-longitude information and the corresponding time of observations.

5.2.2 Estimation of Parameters

The formulas required to accomplish the estimation of parameters have been presented in Sections 3.4.2 and 3.4.3. The specific equations involved are (3-35), (3-37), (3-43), through (3-45) and equation (3-52) with equations (3-49) and (3-51). In addition to the filtered altimetry data, the ground truth geoid data are required to evaluate the vector W as defined in equation (3-35).

The subsatellite points at intervals of five seconds are plotted on the map on which the ground truth geoid (Marsh-Vincent's detailed gravimetric geoid) is given in the form of contours. The corresponding ground truth geoid values are, then, interpolated using these contours. In order to make the constraints between different segments of the profiles corresponding to the different submodes of observations realistic, the first and the last altimeter observations in a segment are included in the bias estimation even though the interval between any of these and the next observation may not be five seconds.

Only the ground truth geoid values obtained as described above and the corresponding altimeter data are input for estimating the biases. The weight matrices defined in equation (3-54) form the rest of the input data in this step. Since the altimetry data is already filtered for noise, they will be more accurate than the ground truth geoid. Consequently, the accuracy estimates assumed are 0.5 meter for the altimetry data and 5.0 meters for the ground truth geoid. The accuracy estimates for the bias term is infinity. With these estimates, the weight matrices become:

$$\begin{aligned} P &= 4.0.I \\ P_{x_1} &= 0.0.I \\ P_{x_2} &= 0.04.I \end{aligned} \qquad (5\text{-}3)$$

With these data, the bias terms have been estimated and the required geoid undulations are obtained by evaluating equation (3-78). This is done not only for the observations used in the estimation procedure, but also for the rest of the observations in the pass. Another set of undulations are obtained

by using the unfiltered altimetry data, N_a, instead of N_a^s in the equation (3-78). These two sets of undulations are, then, punched on cards to be input in the computer program which presents these results in graphical forms along with the ground truth for convenient comparisons and evaluations.

5.3 Results and Analysis

5.3.1 Validation of the Filtering Technique

To test the validity and the degree of smoothing of the filtering technique described earlier, the data in pass #7 were selected due to its low signal to noise ratio. Only those data from each segment were included in simultaneous filtering to minimize the computation effort. The standard deviations of one meter and two meters were assigned for the altimeter data to study their effect on the extent of smoothing.

The results of this filtering are presented in Figures 5-2 and 5-3 where the filtered data are corrected for bias, if any, so that the resulting profiles can be compared with the ground truth geoid profiles. It should also be noted that the various segments of the profiles are not constrained to be continuous.

These figures indicate that, in spite of the low signal to noise ratio in the data, the technique is very effective in filtering the noise from the data. The degree of smoothing changes significantly with the change in σ. Comparing the two figures, it can be noted that the variation in the geoid profile is more realistic in the case where $\sigma \simeq 2$ m. Consequently, it has been decided to keep the value of 2 m for σ for the data in pass #7. However, since the signal to noise ratio, in the data from the other passes is relatively larger than that in pass #7, a value of one meter is used for the other passes.

5.3.2 Processing of the Altimetry Data

The data from EREP passes #4, #6, #7, and #9 have been processed using the formulations and procedures described earlier, the specific ones being the filtering and the estimation. Three solutions, using various

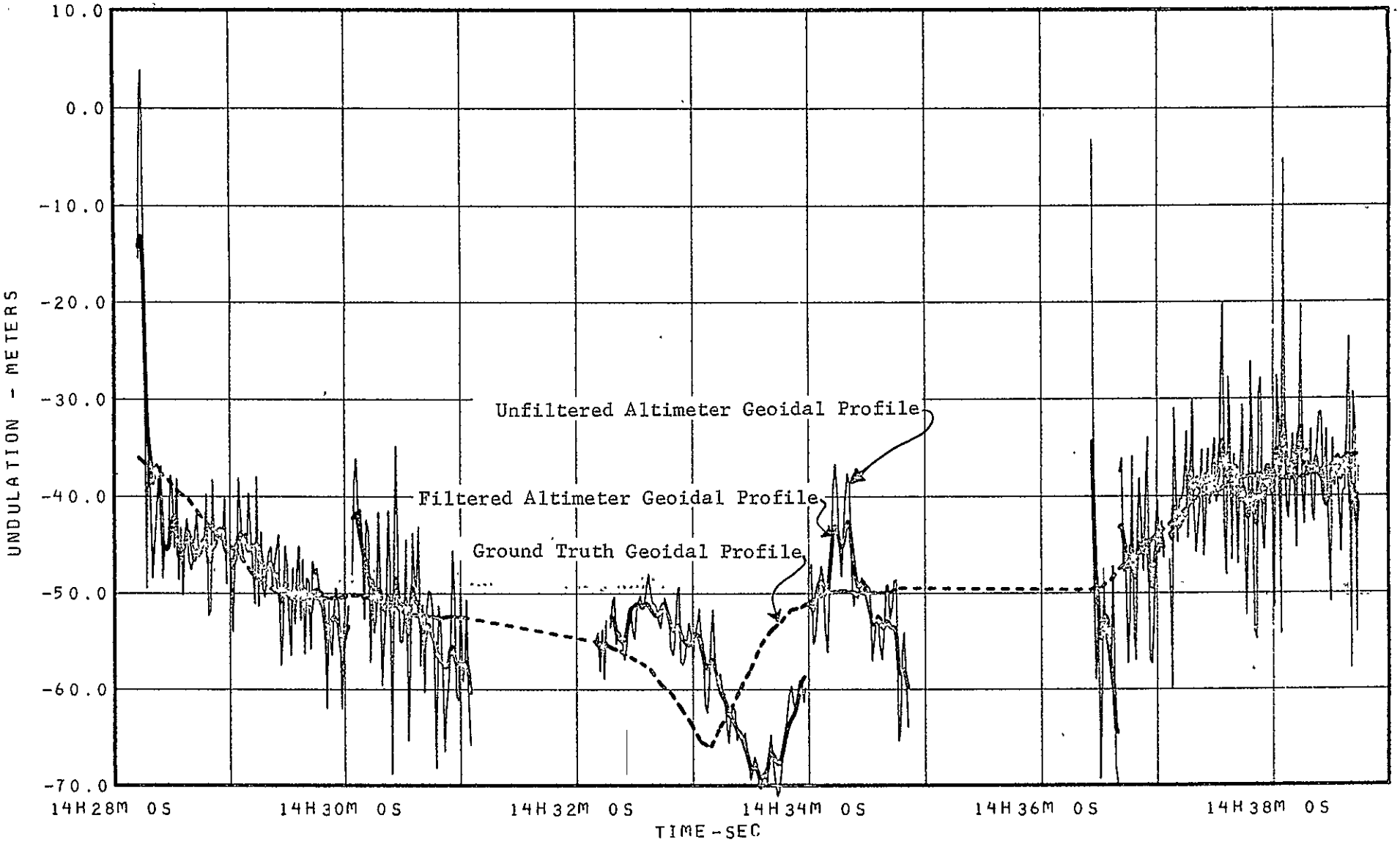

FIGURE 5-2. GEOID UNDULATIONS COMPUTED FROM SKYLAB PASS-7 ALTIMETRY DATA (ALTIMETER PRECISION = 1 m)

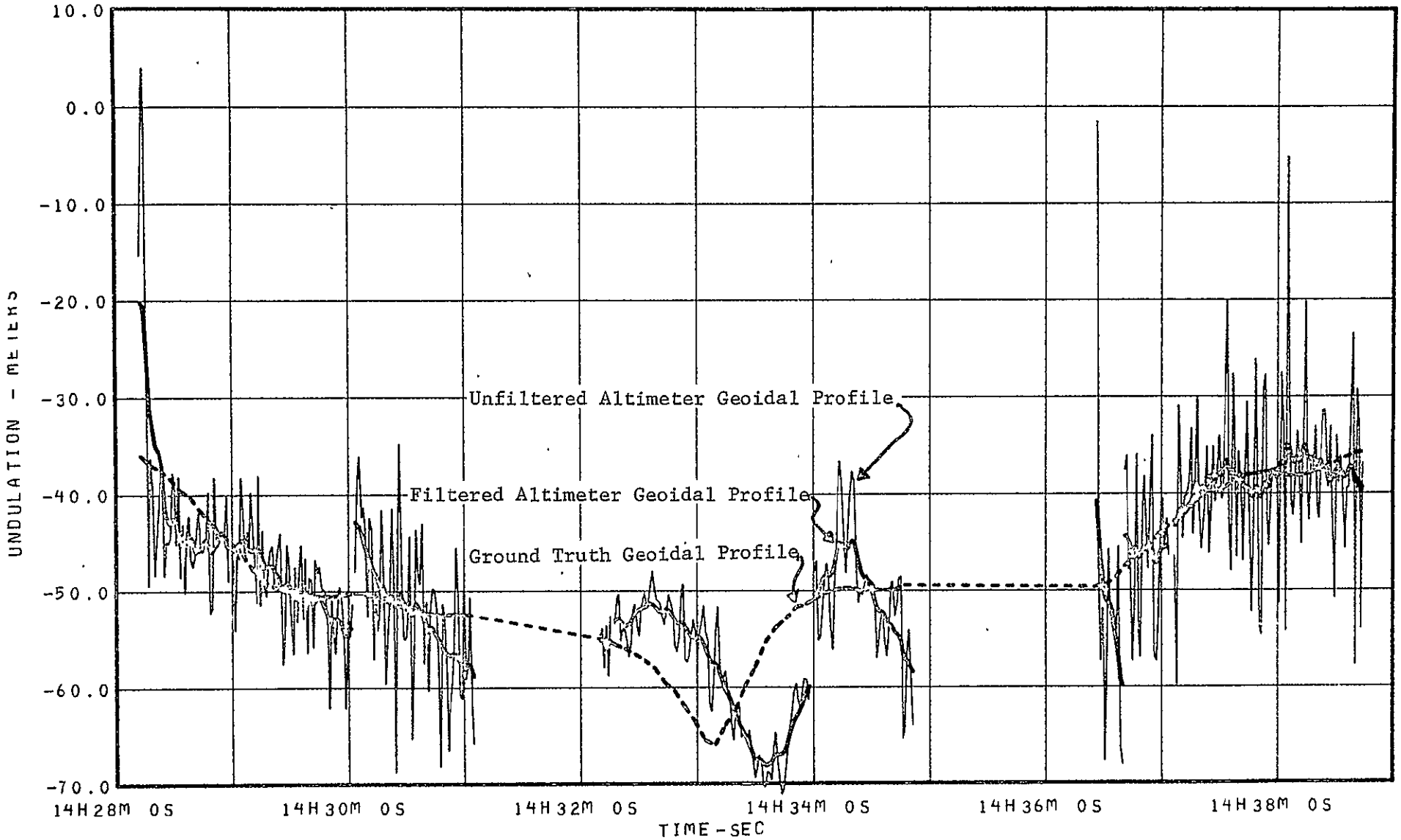

FIGURE 5-3. GEOID UNDULATIONS COMPUTED FROM SKYLAB PASS-7 ALTIMETRY DATA (ALTIMETER PRECISION = 2 m)

combinations of these procedures, have been obtained for the bias terms as follows:

Solution 1: Unfiltered data without constraints.
Solution 2: Filtered data without constraints.
Solution 3: Filtered data with constraints.

The bias terms recovered for various segments of the data are presented in Table 5-2 for all the three solutions. The geoid profiles obtained using the set of bias terms from the third solution are presented graphically as follows:

Pass	Mode	Figure
4	1	5-4
4	5	5-5
6	5	5-6
7	1	5-7
7	5	5-8
7	3	5-9
9	5	5-10
9	3	5-11

In these figures, three geoid, one each of gravity anomaly and one ocean bottom topography profiles are shown. A detailed discussion on the gravity anomaly and bottom topography profiles are presented in Section 6.0. Of the geoid profiles, the ground truth is shown by a dashed line; geoid profiles computed from the unfiltered data using the set of bias terms from the third solution are shown by thin lines while the geoid profiles from the filtered data are shown by thick lines.

From Table 5-2, let the difference between the bias for each segment recovered in Solution 1 and that recovered in Solution 2 be Δ_1. Similarly, let the difference in bias between Solutions 2 and 3 be Δ_2. These differences Δ_1 and Δ_2 are listed in Table 5-3 against their respective profile segments. RMS Δ_1, and RMS Δ_2 are the root mean square values of Δ_1 and Δ_2, respectively, in meters for the segments observed in a single mode and constrained to form continuous profiles.

TABLE 5-2. RESULTS OF THE BIAS RECOVERY FROM ALTIMETRY DATA

Pass	Mode	Submode	Submode*	Unconstrained Bias(m) Unfiltered	Unconstrained Bias(m) Filtered	Constrained Bias(m) Filtered
4	1	0	1	-23·87	-23·99	-23·26
		1	2	- 9·05	- 9·00	-10·25
		2	3	-13·74	-13·59	-12·60
	5	0	7	-33·10	-28·78	-28·12
		1	8	-10·01	- 8·88	- 9·02
6	5	0	1	-22.38	-22·29	-24·03
		1	2	-13.93	-12·61	-11·63
		2	3	- 1.99	- 1·96	- 3·31
7	1	0	1	-53·58	-49·20	-52·43
		1	2	-37.59	-36·37	-40·28
		2	3	-86·17	-84·85	-79·28
	5	0	7	-57·61	-59·05	-63·55
		1	8	-49.49	-49·72	-52·38
		2	9	-52·94	-52·80	-46·56
	3	3	16	-85·09	-79·03	-
		4	17	-87·67	-87·21	-88·87
		5	18	-87·69	-87·77	-87·39
9	5	0	1	-20·80	-19·83	-17·07
		1	2	- 7·27	- 6·58	- 6·07
		2	3	2·81	2·66	0·62
	3	3	10	-16·40	-16·86	-19·99
		4	11	-18·23	-18·13	-20·53
		5	12	-20·00	-20·17	-18·95
		3	18	-31·72	-32·97	-36·95
		4	19	-34·02	-34·03	-36·26
		5	20	-35·98	-35·2	-34·80

TABLE 5-3. DIFFERENCES IN BIAS OBTAINED IN THE VARIOUS SOLUTIONS

Pass	Submode*	Δ_1(m)	RMS Δ_1 (m)	Δ_2(m)	RMS Δ_2 (m)
4	1	-0.1		0.7	
	2	0.0	0.1	-1.2	1.0
	3	0.1		1.0	
	7	4.3	3.0	0.7	0.5
	8	1.1		-0.1	
6	1	0.1		-1.7	
	2	1.3	0.8	1.0	1.4
	3	0.0		-1.4	
7	1	4.4		-3.2	
	2	1.2	2.6	-3.9	4.2
	3	1.3		5.5	
	7	-1.4		-4.5	
	8	-0.2	0.8	-2.7	4.7
	9	0.1		6.2	
	16	6.1		-	
	17	0.4	3.4	1.6	1.1
	18	-0.1		0.4	
9	1	1.0		2.6	
	2	0.7	0.7	0.5	1.9
	3	-0.1		-2.0	
	10	-0.5		-3.1	
	11	-0.1	0.3	-2.4	2.4
	12	-0.2		1.2	
	18	-1.2		-4.0	
	19	0.0	0.8	-2.2	2.6
	20	0.7		0.4	

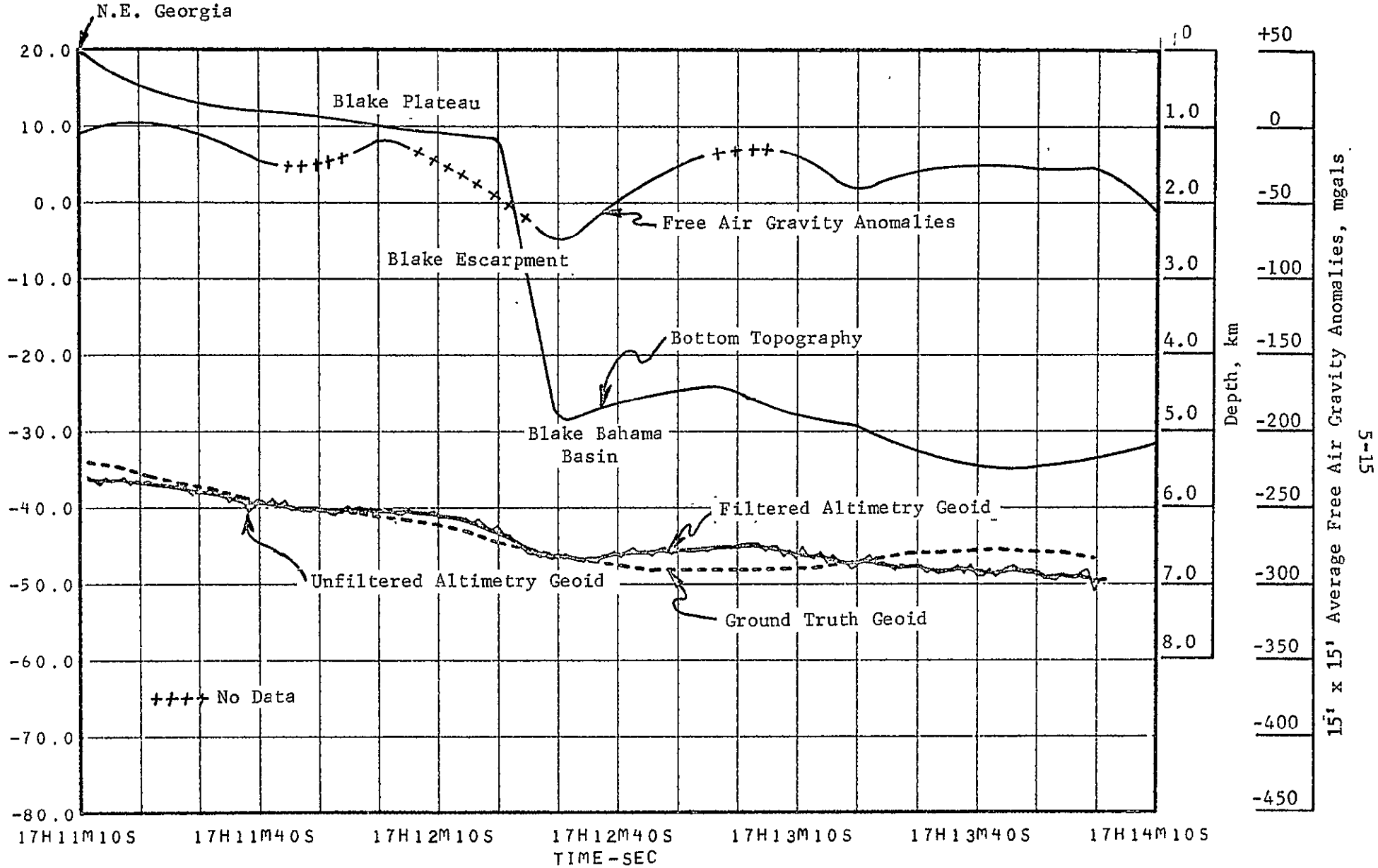

FIGURE 5-4. GEOID UNDULATIONS COMPUTED FROM SKYLAB PASS-4 ALTIMETRY DATA-MODE 1

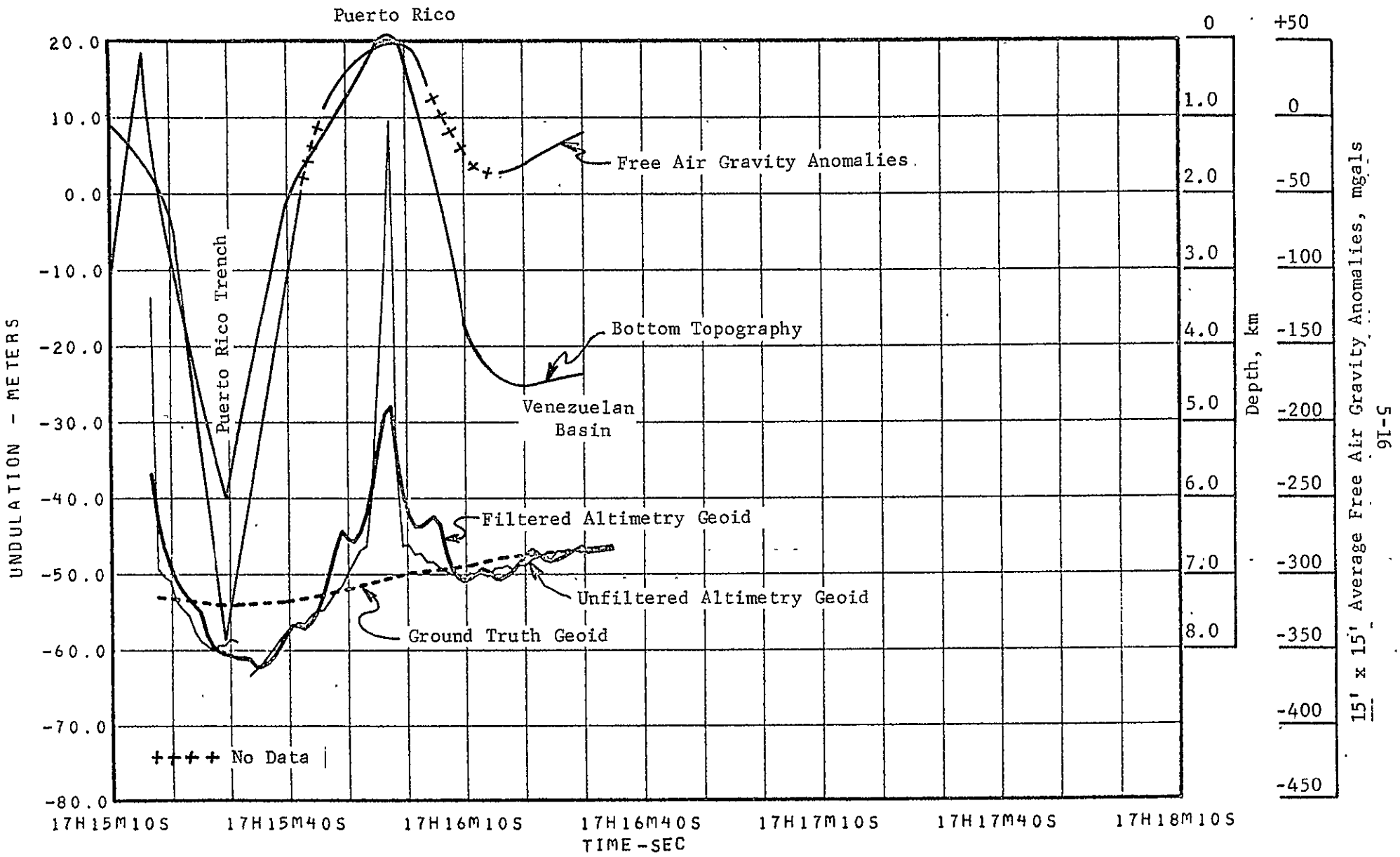

FIGURE 5-5. GEOID UNDULATIONS COMPUTED FROM SKYLAB PASS-4 ALTIMETRY DATA-MODE 5

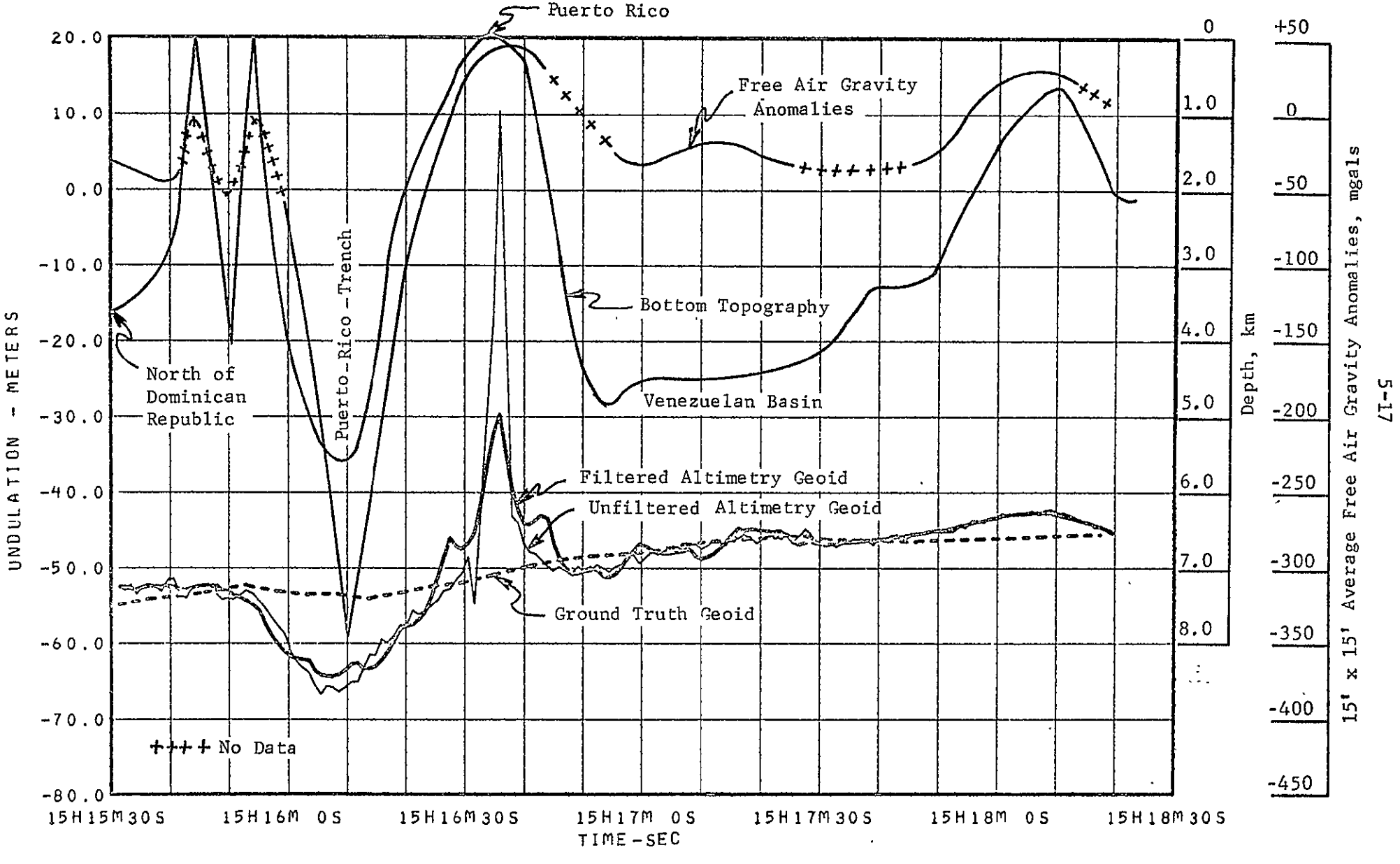

FIGURE 5-6. GEOID UNDULATIONS COMPUTED FROM SKYLAB PASS-6 ALTIMETRY DATA-MODE 5

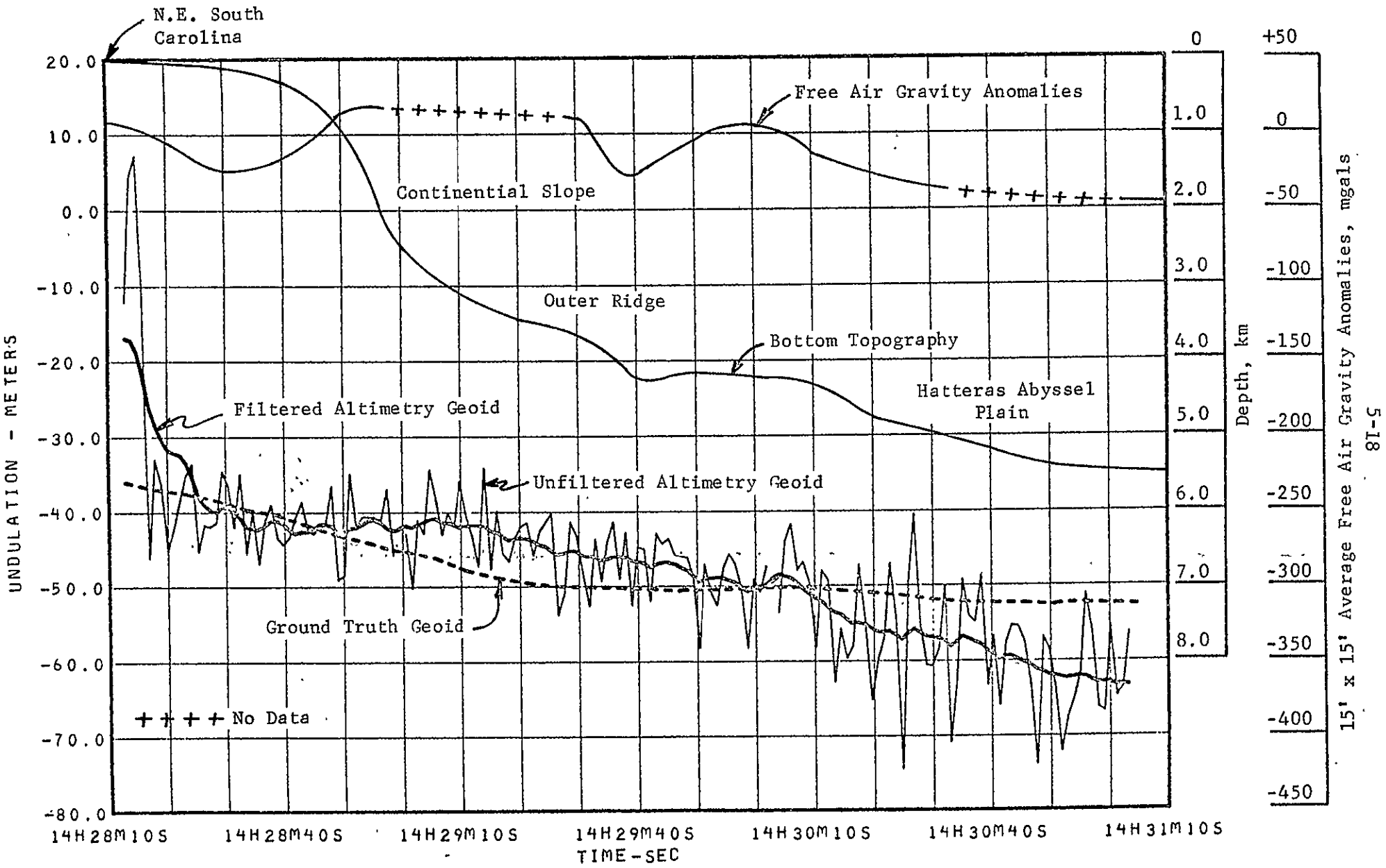

FIGURE 5-7. GEOID UNDULATIONS COMPUTED FROM SKYLAB PASS-7 ALTIMETRY DATA-MODE 1

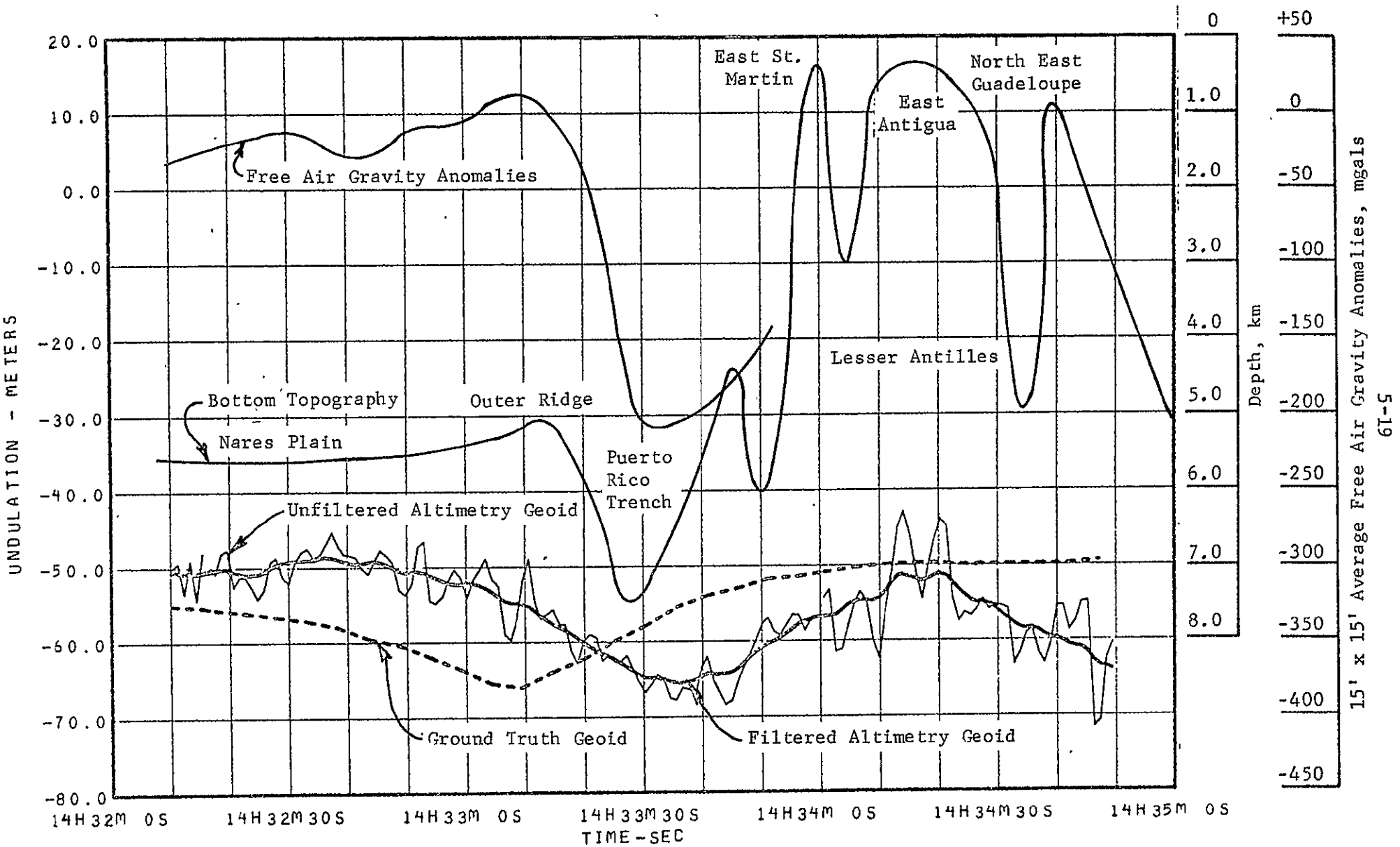

FIGURE 5-8. GEOID UNDULATIONS COMPUTED FROM SKYLAB PASS-7 ALTIMETRY DATA-MODE 5

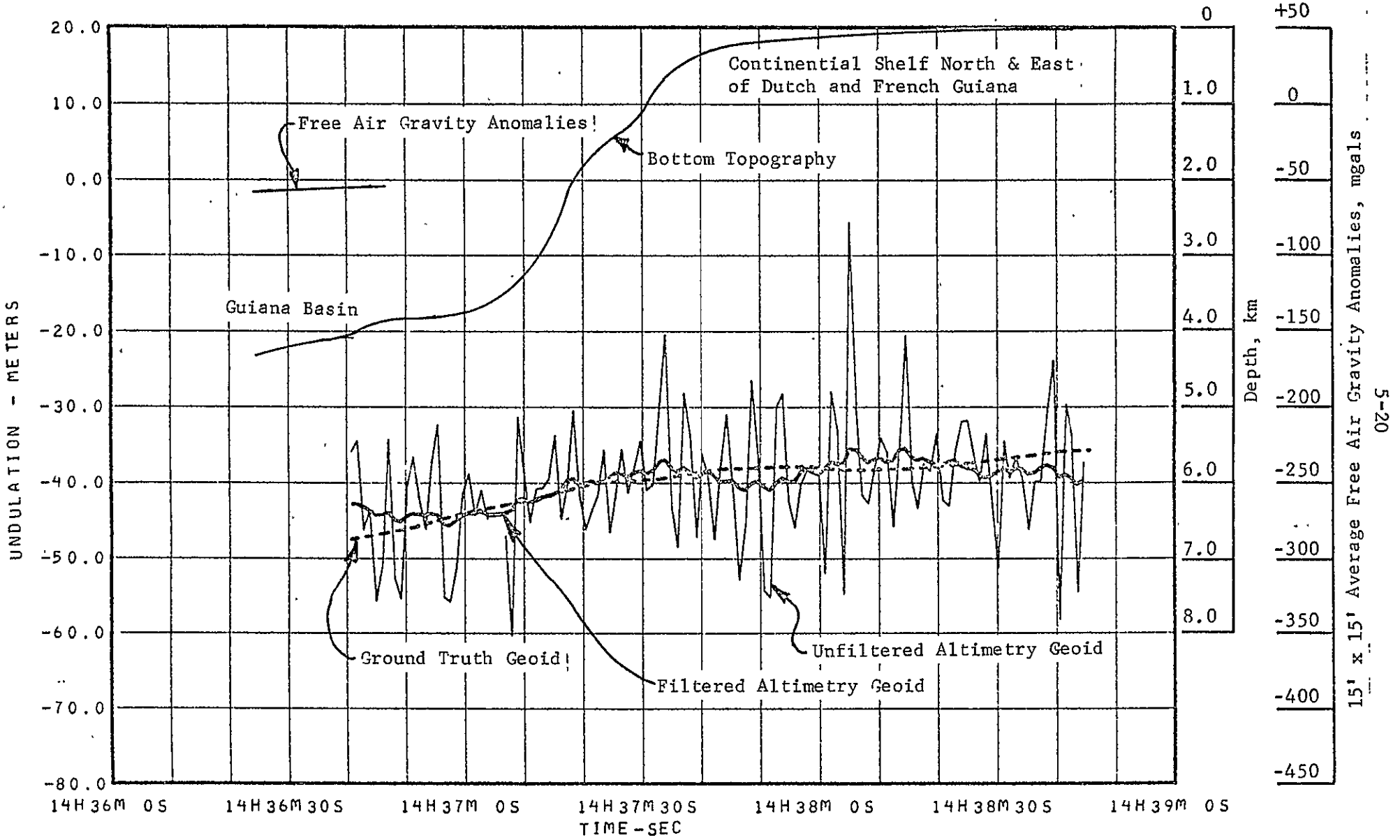

FIGURE 5-9. GEOID UNDULATIONS COMPUTED FROM SKYLAB PASS-7 ALTIMETRY DATA-MODE 3

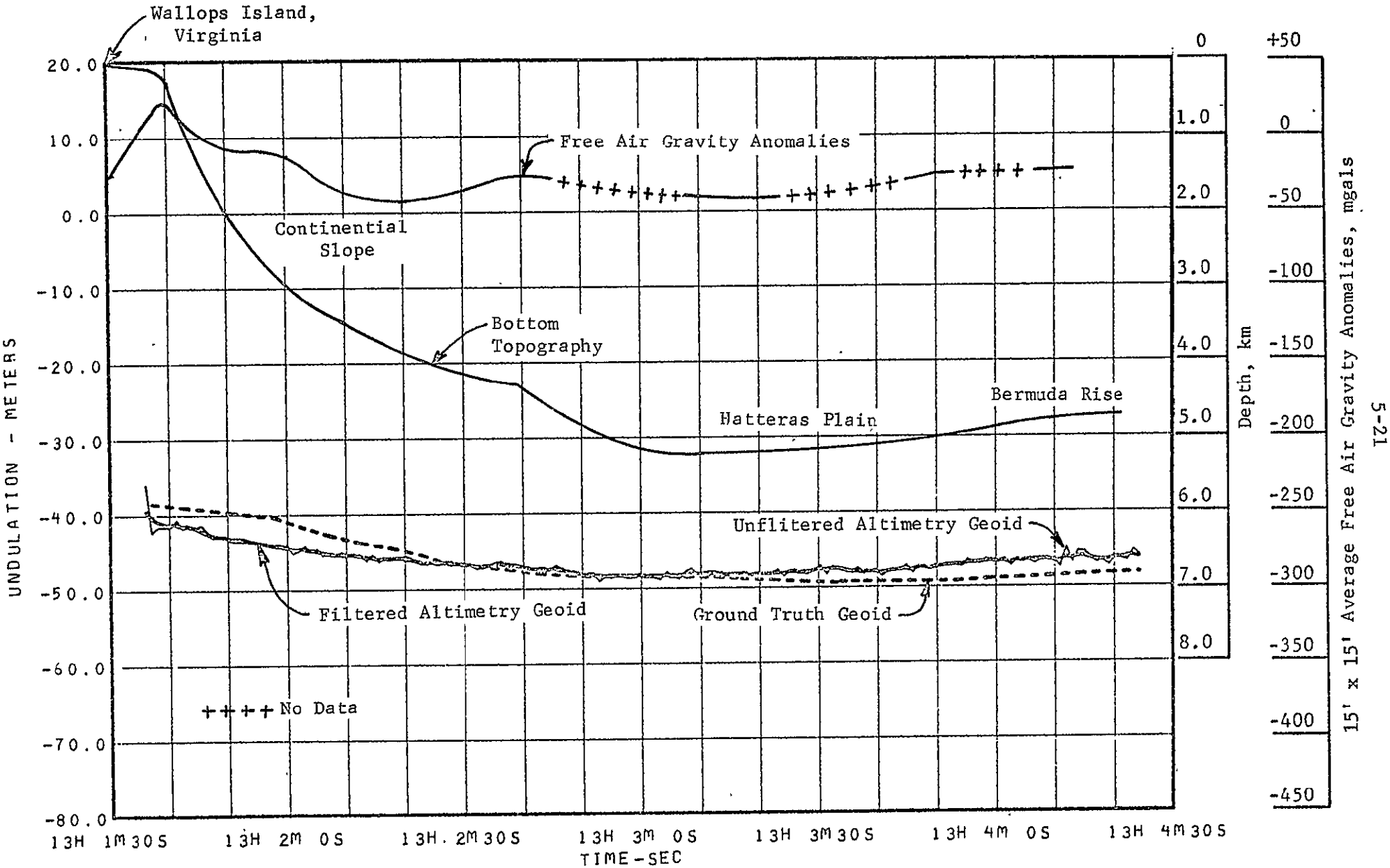

FIGURE 5-10. GEOID UNDULATIONS COMPUTED FROM SKYLAB PASS-9 ALTIMETRY DATA-MODE 5

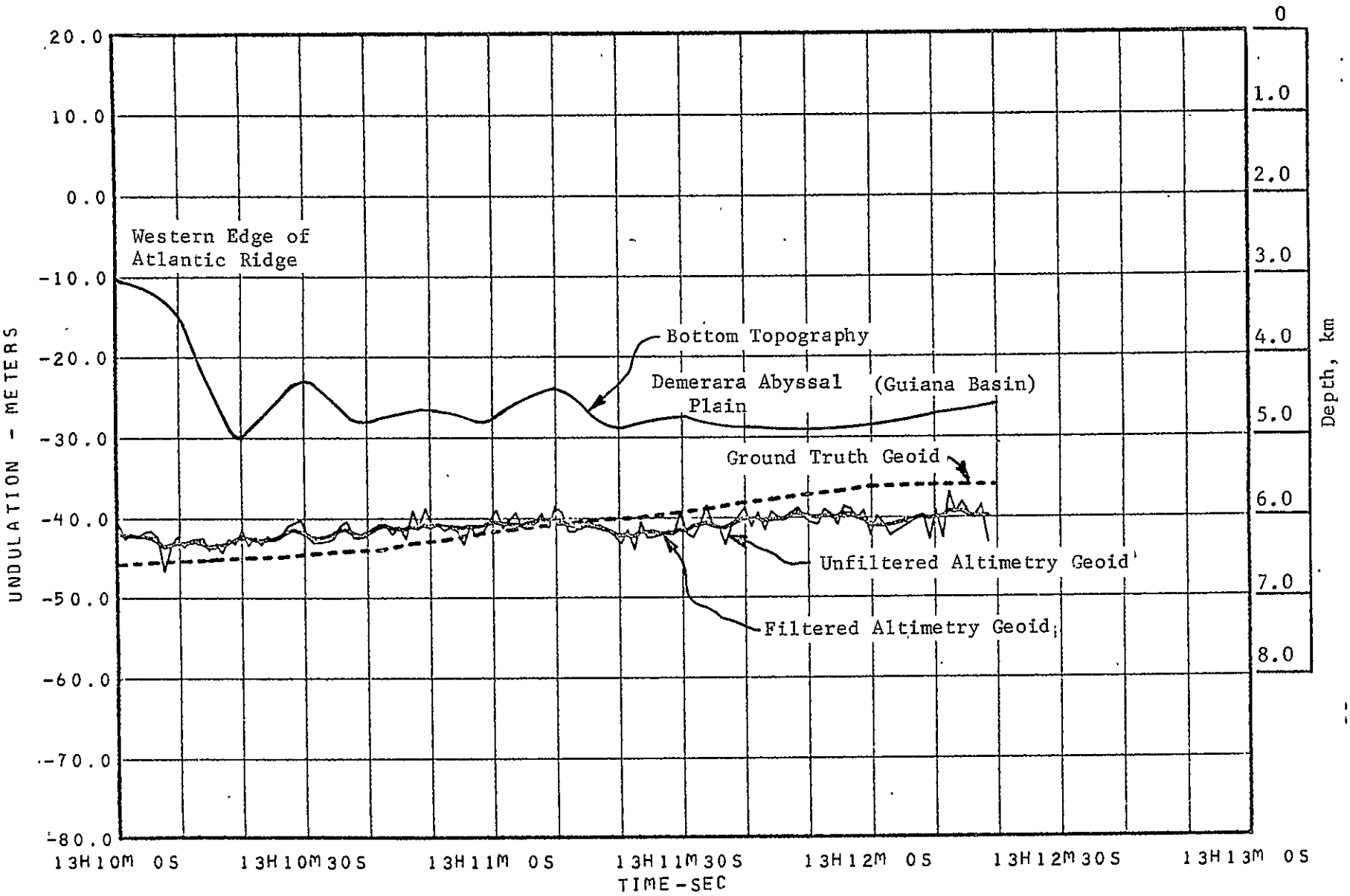

FIGURE 5-11. GEOID UNDULATIONS COMPUTED FROM SKYLAB PASS-9 ALTIMETRY DATA-MODE 3

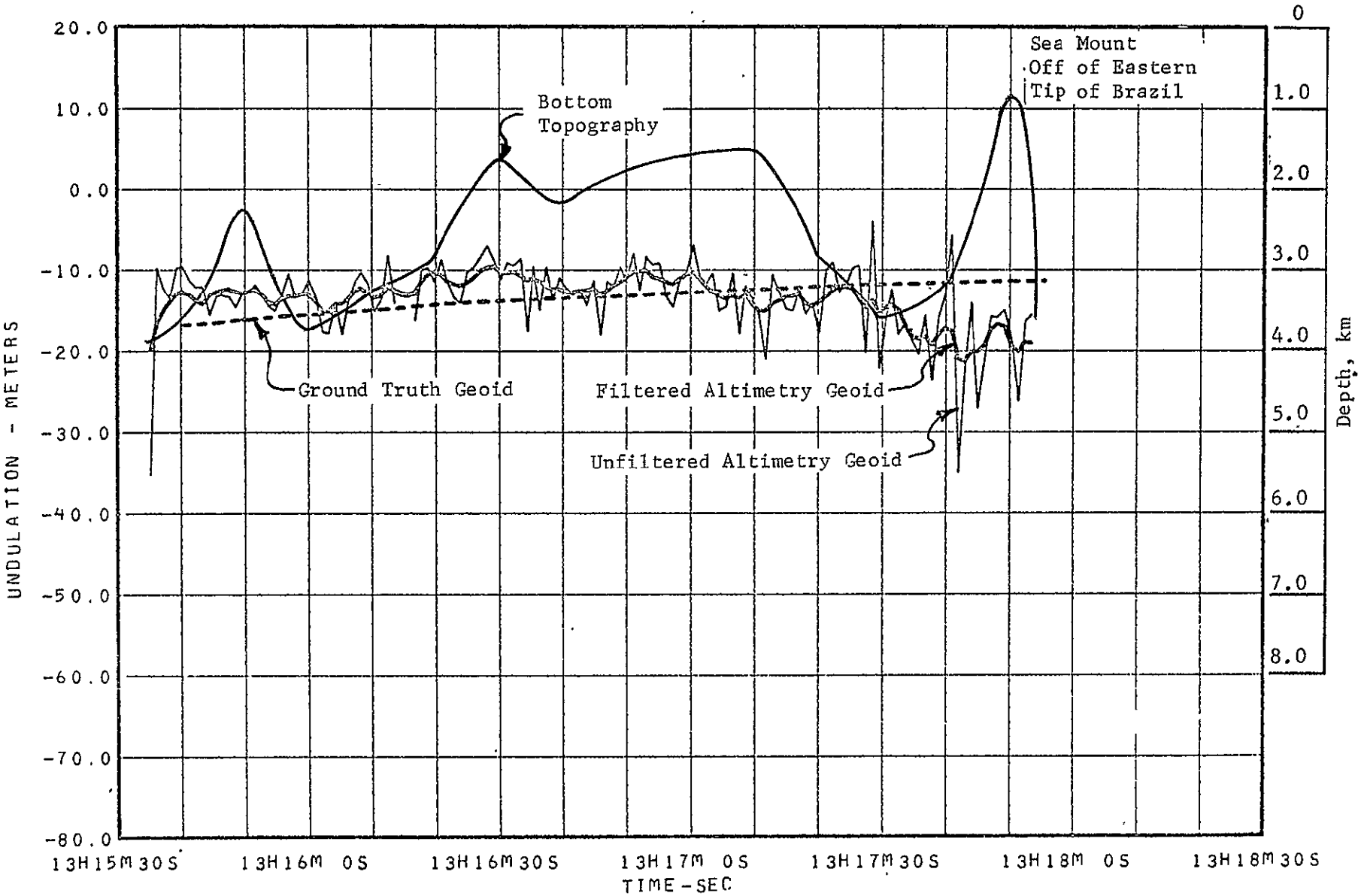

FIGURE 5-11. (con't) GEOID UNDULATIONS COMPUTED FROM SKYLAB PASS-9 ALTIMETRY DATA-MODE 3

The indications, from Table 5-3, are that Δ_1 is small compared to the accuracy levels of both the altimeter and ground truth data. The only exceptions to this are 3 submodes* (submode* 7 in pass #4 and submodes* 1 and 16 in pass #7) which are at the beginning of the modes. The probable cause for this large deviation is due to the errors caused by switching pulse width and band widths and pointing between modes. This observation is well supported by Figures 5-5, 5-7, and 5-9 which show instrument malfunction or instability at the beginning of the modes. The low value of Δ_1 indicates that the filtering removed mostly the random noise and its effects on the systematic bias has been very little. On the other hand, Δ_2's, which are due to the constraints, are significantly large. In spite of these constraints which are absolutely necessary to be realistic, these differences (Δ_2) are relatively high indicating that the ground truth and the altimeter geoid profiles have significant differences. The larger the Δ_2's are, the more significant the differences between these profiles would be. For example, in pass #7 modes 1 and 5 and in pass #9 mode 3, Δ_2 is larger than in the rest of the profiles. This suggests large differences in the ground truth and the altimeter geoid profiles which can easily be seen in the Figures 5-7, 5-8, and 5-11.

Since the altimetry data were fitted to the ground truth geoid in the determination of the bias terms, any scale error in the ground truth would be passed on to the altimetry geoid. Consequently, any deviation of the altimetry geoid profiles from the ground truth profile will be short periodic. In general, the deviation between the two sets of profiles is within about 2-3 meters with the following exceptions: In pass #7 modes 1 and 5 (Figures 5-7 and 5-8) the deviation ranges from 0 to 12 m while it is about 0-8 meters in pass #9 mode 3 (Figure 5-11). In passes #4 and #6 (Figures 5-5 and 5-6), the maximum difference is about 12 m in the Puerto Rican trench area.

A close examination of these differences indicates that these extreme deviations occur in areas of special features such as trenches, ridges and sea mounts. Passes #4 and #6 cross the Puerto Rican trench on the west side. Pass #7 mode 5 is along the western edge of the mid-Atlantic ridge while pass #7 mode 3 corsses the Puerto-Rican trench at the Eastern end. Pass #9 mode 3 is along a range of sea mounts.

These deviations may be due to several causes:

(1) Residual errors due to orbit uncertainties

(2) High frequency component of the geoid not reflected in the ground truth data

(3) Possible (nadir) alignment errors which results in the departure of the sensor field of view from the nadir.

(4) Influence of sea state, tides and ocean circulation effects

(5) Possible inaccuracies in the computation of the ground truth data

(6) Errors introduced as a result of scaling these data off small scale world maps.

Most of the systematic bias caused by the above would be absorbed in the bias terms recovered from the data especially due to the shortness of the segments for which separate bias terms were considered. The short periodic deviations caused by sea-state, tides, ocean circulation effects, etc., would be of the order of about 1-2 m. This leads us to believe that, at least, the larger deviations are due to the short periodic components of the geoid not reflected in the ground truth geoid. This is confirmed by the fact that such deviations occur in the areas of significantly large geoidal features.

Another striking difference noted in these profiles occurs in pass #7 (mode 5) which passes across the Puerto Rican trench (Figure 5-8). The trench, as indicated by both profiles, differs horizontally by about 30 seconds of time which are equivalent to about 240 km. Looking at the gravity anomaly and bottom topography profiles, the altimetry geoid profile appears to be correct. However, further investigations should be carried out in order to determine how a gross discrepancy such as this could have occured.

Crossing of passes #4 and #6 (Figures 5-5 and 5-6) across the Puerto Rican trench and land mass area almost at the same place, has provided an ideal opportunity to compare the results to see the consistency of

the altimeter system in determining the geoid. The overlapping segments of the profiles for these passes are shown superimposed in Figure 5-12. The agreement between the profiles is excellent. The only deviation at the beginning of pass #4 mode 5, is due to the instrument transient response after switching pulse width, beam width and pointing between modes. This agreement indicates that the altimeter system is very stable and consistent.

Before concluding the analysis of the results obtained in this investigation, it is felt that some comments on the results of filtering the altimeter data, are necessary.

As can be seen from the Figure 5-4 through 5-11, the general performance of the filtering technique is excellent with the only exceptions being the Puerto Rican trench and land mass areas. These exceptions may be explained as follows: The signals from the observations to the land mass are not geoid undulations, but are the sum of the orthometric heights and the undulations and are not compatible with the covariance function used. In the trench area where the distortions are relatively small, the undulations are extreme and are not well described by the covariance function which described the average behaviour of the undulations. Further, since all the observations have been weighted equally, there has been a tendency to smooth the extreme observations which results in distortions in the rest of the segment. However, these distortions are not very significant and decrease very fast away from these extreme features. Maximum distortion noticed is about 4-5 meters very near the land mass.

From the results and analysis presented thus far, some general comments/observations and conclusions can be made.

(1) The filtering technique described and applied in this investigation appears very effective in removing the noise present in the altimetry data.

(2) The procedure described and applied for estimating the calibration constants (bias) and geoid undulations has produced very satisfactory and realistic results.

(3) The bias terms recovered for different segments of the same pass are significantly different. There appears to be very little or no correlation among the bias terms associated with the same submodes.

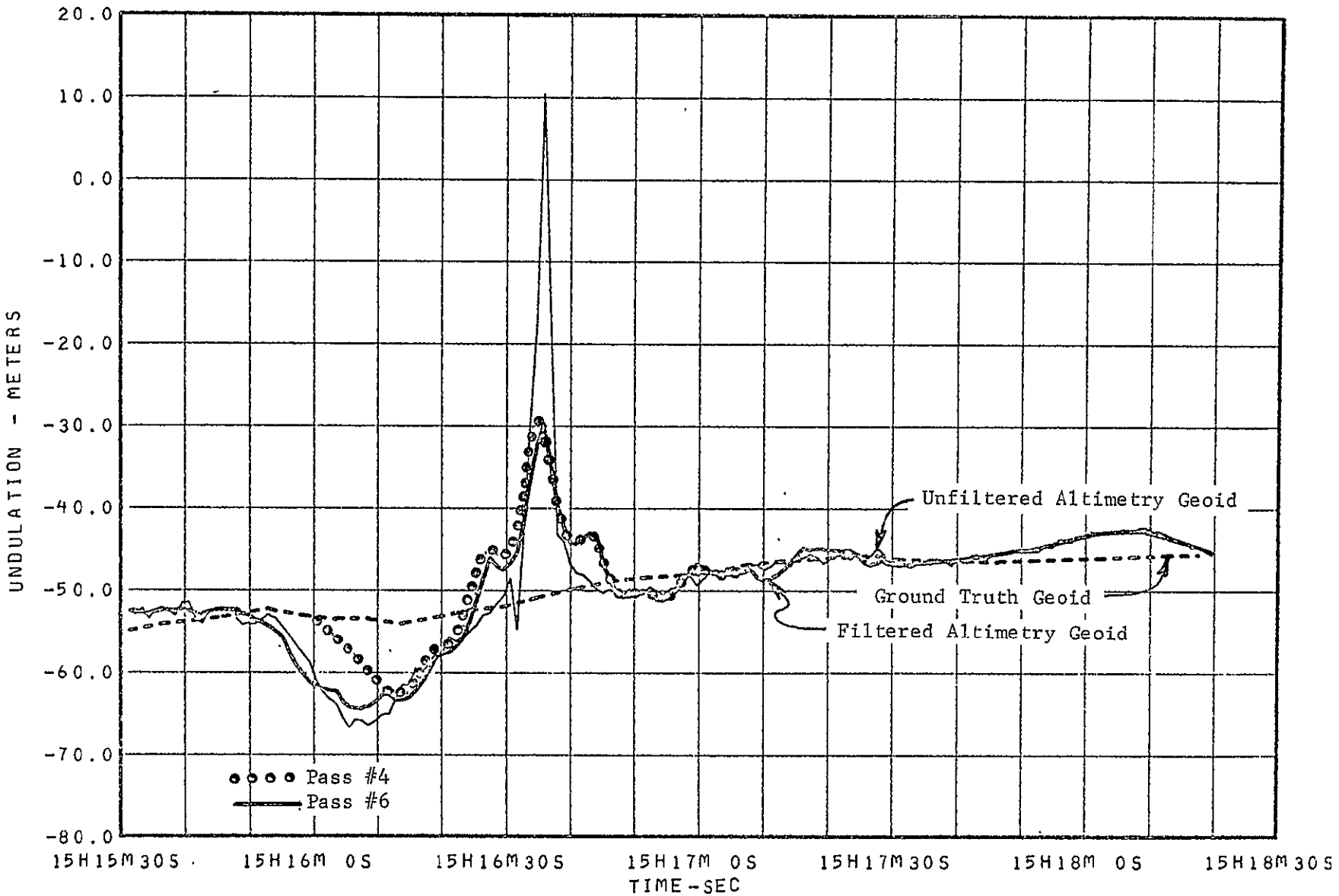

FIGURE 5-12. COMPARISON OF THE ALTIMETRY GEOID PROFILES OVER THE PUERTO RICO TRENCH AND LAND MASS AS OBTAINED IN PASSES 4 AND 6

(4) The agreement between the general slopes of the two geoid (altimetry and ground truth) profiles shows the viability of the altimetry technique in determining the marine geoid.

(5) The magnitude of the deviations of the altimetry geoid from the conventional ground truth leads to the conclusion that these deviations are mostly due to the high frequency components of the geoid rather than due to other causes.

(6) The Skylab altimetry data analyzed here have provided ample evidence that the altimetry sensor is very sensitive to local geoidal features such as trenches, ridges and sea mounts.

(7) Excellent agreement between the results obtained for the same place at different times shows that the satellite altimetry is precise and self consistent except for bias terms.

(8) The correlation between the altimetry geoid and the gravity anomaly and the ocean bottom topography profiles have shown to be useful in verifying major discrepancies in the conventional geoid. These correlations may be also used in other applications such as in geology, geophysics, etc.

6.0 APPLICATIONS OF ALTIMETRY DATA (ALTITUDE)

The applications discussed in this section are concerned with those resulting from the use of altimeter for altitude measurement over the ocean surface which lead to geoid determination. The other applications of altimetry (e.g., measurement of ocean wave heights) are not the subject of this investigation. The use of altimetry for determining the geoid is, perhaps, most significant because of its fundamental applications to geodesy, oceanography, geology, geophysics, navaigation, national defense, environment, resource development and several other applications.

Present methods of determining the geoid depend on the knowledge or measurement of the detailed gravity field all over the earth and the use of satellite perturbations to describe the general field. Measurement of the gravity field all over the earth requires the use of land-based, shipborne, airborne and ocean-bottom gravity instruments. To get worldwide coverage with sufficient accuracy in geoid determination may require something like 20 ships operating continuously for about 20 years to, perhaps, achieve an accuracy of the order of 1-3 m. Present knowledge of the geoid on a worldwide basis is probably not better than 5-30 m at best.

Satellite altimetry offers the most expedient and accurate method for determining the geoid independent of gravity measurements. An accuracy of $\pm$ 10 cm for determining the marine geoid from satellite altimetry is the goal of the NASA's Earth and Ocean Physics Application Program. The results obtained from the Skylab S-193 altimeter experiment proved that the concept is viable. The extent of applications of altimetry data to various disciplines and uses will depend on the degree of accuracy achieved and correlation that can be made between these data and the parameters involved in the application areas. Examples of the results of correlation analyses between the Skylab altimetry-determined geoid, bathymetry and gravity anomalies are discussed next.

6.1 Correlation of Skylab Altimetry Geoid with Bathymetry and Gravity

There are several obvious correlations of the Skylab altimetry-determined geoid with ocean-bottom topography (bathymetry) and surface free air gravity anomalies. Figures 5-4 thru 5-11 show the geoid profile results

of the four Skylab altimetry passes (4, 6, 7, and 9). In addition, these figures show the corresponding ground truth geoidal profiles, the ocean-bottom topographic profiles and the free air gravity anomaly profiles. The results of Pass #4 are shown in Figure 5-4 and 5-5. In Figure 5-4, the altimeter responded clearly to the variation in topography and gravity anomalies caused by the Blake escarpment (about 5 m in geoidal heights, correlated with 3600 m depth changes and about 100 mgals in free air gravity anomalies). Note that the ground truth geoidal profile did not show such a change. The free air gravity anomalies show, also, some correlations with bottom topography over the continental shelf and the Blake plateau. Unfortunately, there are no gravity data (indicated by + + + on the profile) taken at the Blake escarpment. Figure 5-5 shows very strong correlations, over the Puerto Rico Trench, between the altimetry geoid and both the gravity and bathymetry, (about 15 m geoidal height change corresponding to about 6,000 m change in depth and 400 mgal in free air gravity anomalies). Again, note the difference with the ground truth geoid. The altimeter also responded clearly to the land mass as evident by the sharp rise over Puerto Rico.

Pass #6 (Figure 5-6) provided an excellent opportunity to show the repeatability of the altimeter over the Puerto Rico Trench and Puerto Rico as were discussed in Pass #4. The altimeter is perhaps showing some changes due to the shallow water as the Skylab approaches the Lesser Antilles. There is also strong correlation with the gravity. The ground truth geoid is very smooth.

Pass #7 is shown in Figures 5-7, 5-8, and 5-9. While there is significantly high correlation between the gravity anomalies and the bottom topography, there is little correlation with the altimeter geoid. For example, the bottom topography changes gradually over the continental slope to the outer ridge by about 4,000 m. The altimeter geoid did not show the same correlation as was observed over the Blake escarpment for similar depth changes although not as steep. There are also sharp differences between the altimeter and the ground truth geoids. The ground truth geoid, in this case, shows a change in slope corresponding to the continental slope in opposite to the slope indicated by the altimeter geoid. On the other hand, the altimeter geoid shows some correlation with the change in topography from the outer ridge to the Hatteras Abyssal plain. Figure 5-8 shows a strong correlation with the Puerto Rico Trench (this is the eastern end of the trench which is different from those

shown in passes #4 and #6). Also, the rise in the altimeter geoid correlates well with the rise in topography going toward the Lesser Antilles. It appears that the ground truth geoid could be in error here. It would respond to the trench if it is moved by about 200-250 km to the right in Figure 5-8. Figure 5-9 shows slight correlations with bottom topography at the continental slope and some perturbations over the continental shelf that are not indicated by the ground truth geoid. The gravity anomalies are extremely scarce for this segment of the pass.

The results of pass #9 are shown in Figures 5-10 and 5-11. The first segment of pass #9, shown in Figure 5-10, indicates a smooth geoid over the whole profile. The geoid variations do not conform to the bottom topography and gravity particularly over the continental slope. It does correlate with the ground truth geoid, however, with one exception where the ground truth profile shows a slight dip corresponding to the continental slope. The second altimeter profile segment of pass #9 is shown in Figure 5-11. Here, the altimeter geoidal profile exhibits several waves similar to those on the bottom topography porfile. The correlation, if any, is not pronounced since the bottom topographic changes are relatively small (500 m) compared to the other profiles of passes #4, #6, and #7. Also, the third segment of pass #9 has some correlations but they are not pronounced. The last two segments of pass #9 did not have any gravity data available for comparison.

In summary, there are pronounced correlations between the altimeter-determined geoid, the topography and gravity anomaly profiles, particularly those corresponding to special earth structures such as the Puerto Rico Trench. In many cases the altimeter appeared to sense much more details in the geoidal surface than those obtained from the ground truth geoid. There are also some correlations with sea mounts or shallow near-surface topographic features. McGoogan, et al [1974a, 1974b] showed similar correlations with the Puerto Rico Trench and the Mariana Trench. In addition, he showed some correlations with specific sea mounts and the Flemish cap as well as an overall correlation with the ground truth geoid in around-the-world-profile. Our investigation was limited to the data obtained from the four passes discussed in this report.

The causes of different gravity anomaly values, hence geoidal features, associated with different but similar bottom topographic features are due to variations in the mass distribution in the earth crust and mantle, and to the degree of isostatic compensation. In order to realistically determine and evaluate the various deviations associated with the altimetry geoidal passes, more extensive effort is required. Such an effort could entail constructing sub-bottom profiles, based on various density assumptions and additional geophysical data (magnetic, seismic, geologic) and comparing the results with the geoidal profiles.

6.2 Future Altimetry Applications

As mentioned earlier the extent of applications of satellite altimetry will depend to a large extent on the degree of accuracy achieved in the determination of the geoid. With the GEOS-3 satellite altimeter (launched April 1975), a 1-5 m geoid accuracy is expected. By 1978/1979 another altimeter is being planned to fly on SEASAT with sub-meter expected accuracy in geoid determination. Some of the problem areas related to altimetry accuracy which should also be resolved in the future are related to (1) accurate orbit determination, (2) precise altimeter instrumentation, (3) ground truth verification data, (4) methods of interpolating and extrapolating altimetry into unsurveyed areas, and (5) separation of the geoid from other sea surface topographic effects.

The future altimetry applications include the following:

(1) Geodesy /Navigation - Any improvement in the determination of the geoid contributes to geodesy and navigation. With an accuracy of $\pm$ 1 m in geoid determination, many geodetic objectives can be achieved. The major contributions are in improving the determination of the size and shape of the earth and a unified datum and coordinate system on a worldwide basis. Determination of the figure of the earth, until the present, has depended largely on continental data. Satellite altimetry is certain to change that trend and base the figure of the earth on ocean data comprising over 70% of the earth's surface. The objectives of the new adjustment of the North American Datum (NAD) is 1 m. The NAD is used for many civilian applications such as surveying, mapping, engineering operations, navigation and resource development. The extension of control points and determining their three-dimensional

coordinates to offshore areas as well as the determination of national and international marine boundaries must be established in the same system. Accurate knowledge of absolute deflection of the vertical at sea, if combined with marine geodetic control could provide the orientation required for all national datums. These absolute deflections are important for improving the accuracy of shipboard inertial navigation systems. Knowledge of the geoid to $\pm$ 10 cm from altimetry could provide a worldwide reference for the vertical datum which should contribute to investigations of land subsidence.

(2) Gravity Field Determination - The gravity field can be derived from satellite altimetry. A global solution of a $\pm$ 1 m altimetry geoid could resolve the gravity field to about $1^{o} \times 1^{o}$ which represents about 180 x 180 geopotential model. This resolution will contribute considerably to improving the geopotential model which is used in determination of satellite orbit and missile trajectories. The altimetry geoid could also provide information on the gravity anomalies which in turn are helpful, when combined with other geophysical data, in exploration geophysics and identification of geological structures.

(3) Mean Sea Level (MSL) - A $\pm$ 10 cm geoid will contribute significantly to MSL determination. Computation of direction and magnitude of MSL slopes and the heights of each ocean relative to one another are important and still unresolved problems. These problems are further complicated because the results of geodetic and oceanographic computations of the parameters involved are different from each other. Determination of heights, directions and magnitude of sea level slopes relative to the continents is a key factor in land and environmental use and in studies of the effect of changes in polar ice caps which affect marine life, meteorology and climate.

(4) Plate Tectonics and Ocean Trenches - There is a correlation between the geoid/earth's gravity field and geophysical/geological phenomena required in earth and ocean physics studies. Some of these correlations were shown in Skylab data above. To better understand and model this correlation a knowledge of the fine structures of the ocean geoid is required. Studies of these phenomena contribute to better understanding of continental drift, polar motion and earthquake mechanism.

(5) Oceanography - With a ± 10 cm geoid, it is possible to determine the quasistationary departures of the sea surface topography from the geoid [Apel and Byrne, 1974]. The departures of the sea surface topography from the geoid such as those due to tides, barometric pressures, wind, storm surges have practical applications in the determination of ocean dynamic phenomena such as circulation patterns, mass and nutrient transport, ocean tides, and ocean current influences. Most of these phenomena have important roles in monitoring and preserving the environment, in air-sea interaction and in global numerical weather prediction.

If the above parameters can be referenced to the geoid, satellite altimetry should contribute to their solution on a global basis. For example, sea slopes due to ocean currents could cause local rise of water across the current on the order of 1 meter. Current slopes are proportional to their speed. Therefore, mass transport can be determined. The periodic effect of tides in the open ocean is perhaps on the order of about 1 meter. Its determination is important particularly for the separation of the influence of earth tides. Also barometric pressure could cause variations in the slope of the sea surface up to several meters. Other applications that could be possible are in the prediction of tsunamis (seismic sea wave) and storm surges. These, however, may be detected only if they occur during the pass of the altimetry satellites. Tsunamis amplitudes in the open ocean range, perhaps, from a few centimeters to about 1 meter. They have large wavelengths of the order of several thousand km with about a 1-hour period. Storm surges, which is the local build-up of water due to distant violent storms (such as hurricanes and typhoons), could cause damage and reach wave heights of the order of several meters when they hit coastal areas. Their prediction and direction of movement could be of importance not only for coastal areas but also for maritime ship operations.

The various problems affecting the accuracy of achieving a ± 10 cm geoid must be solved in order to arrive at many of the above applications. The Skylab altimetry experiment, however, has demonstrated proof of concept of geoid determination from altimetry data and that satellite altimetry is a potentially valuable tool having many useful applications. If GEOS-3 and SEASAT achieve their objectives, the impact of altimetry on earth and ocean dynamics studies would be significant.

7.0 REFERENCES

1. Apel, J. R., and Byrne, H. M., "Oceanography and the Marine Geoid", Proceedings of the International Symposium on Applications of Marine Geodesy, pp. 59-66, Marine Technology Society, Washington, D. C., 1974.

2. Decker, B. L., "Present Day Accuracy of the Earth's Gravitational Field", Presented at the International Symposium on Earth Gravity Models and Related Problems, Defense Mapping Agency Aerospace Center, St. Louis Air Force Station, Missouri, August, 1972.

3. Fischer, I., et al, "New Pieces in the Picture Puzzle of an Astrogeodetic Geoid Map of the World", Bulletin Geodesique, No. 88, p. 199, 1968.

4. Fubara, D. M. J., "Three-Dimensional Geodesy Applied to Terrestrial Networks", Ph.D. Dissertation, University of New Brunswick, Fredericton, 1969.

5. Fubara, D. M. J., "Geodetic Numerical and Statistical Analysis of Data", Bulletin Geodesique, No. 108, June, 1973.

6. Fubara, D. M. J., and Mourad, A. G., "Requirements for a Marine Geoid Compatible with Geoid Deducible from Satellite Altimetry", Proceedings of NOAA/NASA/NAVY Conference on Sea Surface Topography from Space, Edited by J. Apel, NOAA TR ERL 228-AOML7, 1972a.

7. Fubara, D. M. J., and Mourad, A. G., "Marine Geodetic Control for Geoidal Profile Mapping Across the Puerto Rican Trench", NASA Wallops Flight Center Contractor Report, NASA CR-141396, March, 1975, Prepared under Contract Number NAS6-2006, April, 1972b.

8. Fubara, D. M. J., and Mourad, A. G., "Applications of Satellite and Marine Geodesy to Operations in the Ocean Environment", NASA Wallops Flight Center Contractor Report No. CR-141395, March, 1975, Prepared under Contract No. NAS6-2006, March, 1973.

9. Gopalapillai, S., "Non-Global Recovery of Gravity Anomalies from a Combination of Terrestrial and Satellite Altimetry Data", Reports of the Department of Geodetic Science, #210, The Ohio State University, Columbus, Ohio, July, 1974.

10. Heiskanan, W. A., and Moritz, H., Physical Geodesy, W. H. Freeman & Co., San Francisco, California, 1967.

11. Kaula, W. M. (Chairman), "The Terrestrial Environment: Solid Earth and Ocean Physics", Report of a Study at Williamstown, Massachusetts, to NASA, Report NASA CR-1579, April, 1970.

12. Kern, R. J., and Katucki, R. J., "S-193 Microware Radiometer/Scatterometer Altimeter, Calibration Data Report, Flight Hardware", Volumes 1B, Rev. D, from General Electric for NASA, March, 1973.

13. Khan, M. A.,"Equatorial Radius of the Earth: A Dynamical Determination", Bull. Geod., 109, 227, 1973.

14. Marsh, James G., and Vincent, Samir, "Global Detailed Geoid Computation and Model Analysis", GSFC Report No. X-921-74-131, Greenbelt, Maryland, 1973.

15. McGoogan, J. T., Wells, W. T., and Miller, L. S., "Skylab Altimeter Applications and Scientific Results". Paper Presented at the AIAA/AGU Conference on Scientific Experiments of Skylab, Huntsville, Alabama, October 30 - November 1, 1974a.

16. McGoogan, J. T., Leito, C. D., Miller, L. S., and Wells, W. T., "Skylab S-193 Altimeter Experiment Performance, Results and Applications", Proceeding of the International Symposium on Applications of Marine Geodesy, pp. 291-300, Marine Technology Society, Washington, D. C., 1974b.

17. Moritz, Helmut, "Advanced Least Squares Methods", Reports of the Dept. of Geodetic Science, No. 175, The Ohio State University, Columbus, Ohio, 1972.

18. Mourad, A. G., Fubara, D. M., Hopper, A. T., and Ruck, G. T., "Geodetic Location of Acoustic Ocean-Bottom Transponders from Surface Positions", E&S, Trans. AGU, Vol. 53, No. 6, 1972a.

19. Mourad, A. G., and Fubara, D. M. J., Interaction of Marine Geodesy, Satellite Technology and Ocean Physics, NASA Wallops Flight Center, Contractor Report NASA CR-137470, Prepared under Contract NAS6-2006, June, 1972v.

20. Mueller, I. I., and Rockie, J. D., Gravimetric and Celestial Geodesy, Frederick Ungar Pub. Co., New York, 1966.

21. Paul, M. K., "A Note on Computation of Geodetic Coordinates from Geocentric (Cartesian) Coordinates", Bulletin Geodesique, No. 108, June, 1973.

22. Rapp, R. H., "Accuracy of Potential Coefficients Determinations from Satellite Altimetry and Terrestrial Gravity", Department of Geodetic Science Report No. 166, The Ohio State University, 1971.

23. Rapp, R. H., "Accuracy of Geoid Undulation Computations", J. Geophys. Res., 78, 7589-7595, 1973.

24. Schmid, H. H., and Erwin Schmid, "A Generalized Least Squares Solution for Hybrid Measuring Systems", 2nd Geodesy Symposium, University of New Brunswick, Fredericton, 1964.

25. Stanley, H. R., and McGoogan, J. T., "The Skylab Radar Altimeter", Proceedings of NOAA/NASA/NAVY Conference on Sea Surface Topography from Space, Edited by J. Apel, NOAA TR ERL 228-AOML7, 1972.

26. Strange, W. E., Vincent, S. E., Berry, R. H., and Marsh, J. G., "A Detailed Gravimetric Geoid for the United States", NASA Preprint, X-552-71-219, 1971.

27. Sturges, W., "Comments on Ocean Circulation with Regard to Satellite Altimetry", Proceedings of NOAA/NASA/NAVY Conference on Sea Surface Topography from Space, Edited by J. Apel, NOAA TR ERL 228-AOML7, 1972.

28. Talwani, M., Poppe, H. R., and Radinowitz, R. D., "Gravimetrically Determined Geoid in the Western North Atlantic", Proceedings of NOAA/NASA/NAVY on Sea Surface Topography from Space, Edited by J. Apel, 1972.

29. Tscherning, C. C., and Rapp, R. H., "Closed Covariance Expressions for Gravity Anomalies, Geoid Undulations and Deflections of the Vertical Implied by Anomaly Degree Variance Models", Reports of the Dept. of Geodetic Science, No. 208, The Ohio State University, Columbus, Ohio, 1974.

30. Veis, G., "The Determination of the Radius of the Earth and other Geodetic Parameters as Derived from Optical Satellite Data", SAO, SR. 264, 1967.

31. Vincent, S., Strange, W. E., and Marsh, J. G., "A Detailed Gravimetric Geoid of North American, North Atlantic, Eurasia, and Australia", Paper Presented at the International Symposium on Earth Gravity Models and Related Problems St. Louis, Missouri, August, 1972.

32. Vincent, S., and Marsh, J. G., "Global Detailed Gravimetric Geoid", Computer Sciences Corporation and NASA/GSFC, Greenbelt, Md., 1973.

33. Wollenhaupt, W. R., and Schiesser, E. R., "Status of Skylab SL-2 EREP Skylab Tapes", FM85 (73-241), Mathematical Physics Branch, NASA/JSC, Houston, Texas, October, 1973.

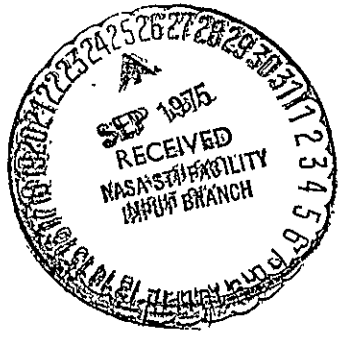
SEP 1975
RECEIVED
NASA STI FACILITY
INPUT BRANCH